HEFAT2014
10th International Conference on Heat Transfer, Fluid Mechanics and Thermodynamics
14 – 16 July 2014
Orlando, Florida

ON CONSERVATION OF SCATTERED ENERGY AND ANGLE IN RADIATIVE TRANSFER COMPUTATIONS

Zhixiong Guo* and Brian Hunter
*Author for correspondence
Department of Mechanical and Aerospace Engineering,
Rutgers, the State University of New Jersey
98 Brett Road,
Piscataway, NJ 08854, USA
E-mail: guo@jove.rutgers.edu

ABSTRACT

To compute accurately radiative transfer in anisotropically-scattering media, conservation of both scattered energy and angle after discretization is required. Alteration of asymmetry factor (i.e., average cosine of scattering angles) due to angular discretization leads to a third type of numerical error, named as angular false scattering. The error that was known as "false scattering" is actually caused by spatial discretization and has nothing to do with scattering; and thus, it is more appropriate to be called "numerical smearing". Five phase-function normalization techniques, designed to attempt to conserve scattered energy, angle, or both, are analyzed here using DOM and FVM for both diffuse and ballistic radiation, to determine their capability to mitigate errors and produce accurate radiative transfer. Comparisons with Monte Carlo benchmark predictions are used to gauge accuracy. The two normalization techniques that conserve both scattered energy and asymmetry factor simultaneously are found to result in substantial improvements in radiative transfer accuracy with respect to MC predictions and comparison to each other. Normalization for ballistic radiation situations is shown to be crucial. Normalization impacts FVM and DOM in similar manners, as the accuracy of both is equal. In terms of computational efficiency, it is found that the DOM is more efficient than the FVM when both have the same number of angular directions.

INTRODUCTION

In engineering problems where radiation is the dominant mode of heat transfer, such as high-temperature combustion and material processing [1-11], fire [12-15] and atmospheric radiation [16-19], renewable solar energy [20-22], space exploration [23-25], microwave and laser applications [26-38], accurate and complete solutions of the governing equation of radiative transfer (ERT) are desired. The integro-differential nature of the ERT makes analytical solution difficult [4, 5], and thus numerical methods, such as the finite volume method (FVM) [39-45] and discrete-ordinates method (DOM) [45-49], are preferred. Numerical methods have garnered increasing attention in the field of radiation heat transfer, as they provide cost-effective alternatives to costly experimentation and their efficiency and accuracy has been improved with the advance of computational technology.

NOMENCLATURE

c	Speed of light in medium
g	Asymmetry factor
I	Radiative intensity (W/m^2sr)
I^B	Ballistic irradiance (W/m^2)
M	Total number of directions
$N_{s\phi}, N_{s\theta}$	Solid angle sub-divisions in azimuthal and polar direction
$\hat{\boldsymbol{n}}$	Surface outward unit normal vector
$\boldsymbol{r}$	Position vector
$\hat{\boldsymbol{s}}$	Unit direction vector
t	Time
Greek Symbols	
σ_a	Absorption coefficient (m^{-1})
σ_s	Scattering coefficient (m^{-1})
Φ	Scattering phase function
$\tilde{\Phi}$	Normalized scattering phase function
ϕ	Radiation direction azimuthal angle (°)
Θ	Scattering angle (°)
θ	Radiation direction polar angle (°)
Subscripts	
b	Blackbody
HG	Henyey-Greenstein
i	Control-volume face
Superscripts	
B	Ballistic
$'$	Radiation incident direction
l, l'	Radiation directions
$l'l$	From direction l' into direction l

Ray effects [50,51] and false scattering [51-53] are two well-known numerical errors associated with DOM. However, they also exist in all discretization-based numerical methods including the FVM. The so-called false scattering was actually the numerical error due to spatial discretization in the dimension domain – similar to artificial diffusion in CFD. Therefore, it would be better to call it as numerical smearing [54], because directional discretization in the solid-angle domain generates the real-meaning false scattering effect [55-59]. Thus, there are three basic types of numerical discretization errors in radiation transfer computation, namely, ray effect, numerical smearing, and angular false scattering.

During numerical computations of radiative heat transfer, it is well known that the scattered energy after angular discretization must be conserved [60-63]; but less known is the preservation of scattering direction [55-57]. Only recently it was discovered that angular discretization would result in change in the physical property of asymmetry factor [55-59,62], which is the average cosine of scattering angle. To correct this issue, one approach is phase-function normalization, which was commonly adopted for conserving scattered energy. Normalization of scattering phase functions must now satisfy two constraints – preservation of average consine of scattered angles (asymmetry factor) and conservation of scattered energy [55].

In this Keynote lecture, we will systematically discuss and compare five normalization techniques to gauge the importance of appropriate phase-function normalization and the possible issues associated with each approach. The applicability of each phase-function normalization technique will be examined using the DOM and FVM. The results will be compared with Monte Carlo predictions in literature. Both Henyey-Greenstein and Legendre polynomial phase functions will be taken into account. Diffuse as well as ballistic radiation will be considered. A recommendation will be made based on the research. Additionally, a comparison of the computational efficiency of both the DOM and FVM is presented.

EQUATION OF RADIATIVE TRANSFER

In general vector notation, the time-dependent ERT of intensity I for a diffuse, gray, and absorbing-emitting-scattering medium can be expressed as follows:

$$\frac{1}{c}\frac{\partial I(\boldsymbol{r},\hat{\boldsymbol{s}},t)}{\partial t}+\hat{\boldsymbol{s}}\cdot\nabla I(\boldsymbol{r},\hat{\boldsymbol{s}},t)=-(\sigma_a+\sigma_s)I(\boldsymbol{r},\hat{\boldsymbol{s}},t)+\sigma_a I_b(\boldsymbol{r},t)+\frac{\sigma_s}{4\pi}\int_{4\pi} I(\boldsymbol{r},\hat{\boldsymbol{s}}',t)\Phi(\hat{\boldsymbol{s}}',\hat{\boldsymbol{s}})d\Omega' \quad (1)$$

In Eq. (1), $I(\boldsymbol{r},\hat{\boldsymbol{s}},t)$ is radiant intensity at a given spatial location $\boldsymbol{r}$ and time t propagating in direction $\hat{\boldsymbol{s}}$, σ_a and σ_s are the absorption and scattering coefficients, respectively, and c is the speed of light in the medium. The terms on the left-hand side represent the temporal and spatial gradients of radiative intensity, while the three terms on the right-hand side are (1) intensity attenuation due to medium absorption and out-scattering, (2) intensity augmentation due to blackbody emission (which is generally negligible for strong laser radiation transport), and (3) intensity augmentation due to radiant in-scattering. The addition of the temporal derivative represents wave propagation of radiant energy at the speed of light. Eq. (1) is integro-differential, in nature, and is a hyperbolic wave equation, making analytic solution almost impossible.

Discretization Using the Discrete Ordinates Method

Using the 3-D Cartesian coordinate system, Eq. (1) can be expanded into a simultaneous set of partial differential equations in discrete radiation directions $\hat{\boldsymbol{s}}^{\boldsymbol{l}}$ using the DOM as follows:

$$\frac{1}{c}\frac{\partial I^l}{\partial t}+\mu^l\frac{\partial I^l}{\partial x}+\eta^l\frac{\partial I^l}{\partial y}+\xi^l\frac{\partial I^l}{\partial z}=-(\sigma_a+\sigma_s)I^l+\sigma_a I_b+S^l \quad (2a)$$

$$S^l=\frac{\sigma_s}{4\pi}\left[\sum_{l'=1}^{M} w^{l'}\Phi^{l'l}I^{l'}+\sum_{B}\Phi^{l^B l}I^B\right] \quad (2b)$$

where $l = 1,2,\ldots,M$. The continuous angular variation of radiation scattering is discretized, using the DOM, into M total radiation directions, where each direction is defined using polar angle θ, azimuthal angle ϕ, and direction cosines μ, η, and ξ. Using the DOM, the integral term in Eq. (1) is replaced by two discrete quadrature summations in Eq. (2b), which represent the in-scattering of both diffuse and ballistic radiation, respectively. The ballistic summation is crucial to include for applications involving irradiation of collimated laser or solar incidence. In the two summations, $w^{l'}$ is the DOM directional weighting factor corresponding to radiation direction $\hat{\boldsymbol{s}}^{\boldsymbol{l'}}$, $\Phi^{l'l}$ is the discrete scattering phase-function for diffuse radiation between two arbitrary radiation directions, I^B is the radiative heat flux of the ballistic radiation at a particular spatial and temporal location, and $\Phi^{l^B l}$ is the discrete scattering phase-function for ballistic radiation between the direction of ballistic incidence and discrete direction $\hat{\boldsymbol{s}}^{\boldsymbol{l}}$.

In order to solve Eq. (2) using the DOM, the computational domain of interest is divided into control volumes, and the spatial derivatives are approximated using the finite volume approach. A DOM quadrature scheme that defines the angular discretization and corresponding discrete direction weighting factors while satisfying directional moment conditions must be chosen. One of the more commonly implemented DOM quadratures is the level-symmetric S_N quadrature, where the subscript N relates to the number of discrete directions as $M = N(N+2)$. This traditional quadrature has a built-in directional limit [64]. To combat this limitation, several high-order quadrature schemes with no directional limitation, such as the EO_N even-odd quadrature [65], EQ_N equal weight quadrature [66], P_N-T_N Legendre-Chebyshev quadrature [64], and the geometric T_N [67] and $SRAP_N$ quadratures [68], were developed. Recently Hunter and Guo [69] compared the above-mentioned schemes and found that while the higher-order quadrature sets are able to effectively minimize ray effect and angular false scattering, the number of directions required is extremely large, and thus it is more

computationally efficient to implement proper phase-function normalization to obtain accurate results

After determination of computational grid, quadrature scheme, and medium properties, Eq. (2) can be solved using a control-volume marching procedure. Further details on DOM solution procedure are not repeated here, for brevity, but are readily available in the authors' previous publications [48,49].

Discretization Using the Finite Volume Method

Using a control volume approach, Eq. (1) can be integrated over an arbitrary spatial control volume ΔV and discrete solid angle $\Delta\Omega^l$, where the discrete radiation direction $\hat{\boldsymbol{s}}^{\boldsymbol{l}}$ denotes the centroid of solid angle $\Delta\Omega^l$ [39]. After integration, and application of Gauss' theorem to transform volume integrals into surface area integrals, the discretized form of Eq. (1) for the FVM becomes:

$$\frac{1}{c}\frac{\partial I^l}{\partial t}\Delta V\Delta\Omega^l + \sum_i I_i^l A_i D_i^l = -(\sigma_a + \sigma_s)I^l\Delta V\Delta\Omega^l + S^l\Delta V\Delta\Omega^l \tag{3a}$$

$$S^l = \sigma_a I_b + \frac{\sigma_s}{4\pi}\left(\sum_{l'=1}^{M}\overline{\Phi}^{l'l} I^{l'}\Delta\Omega^{l'} + \sum_B I^B\Phi^{Bl}\right) \tag{3b}$$

where l = 1,2,…,M. The use of a summation over the control volume faces i to approximate the spatial gradient of radiative intensity follows the assumption that intensity at any location inside a control volume and solid angle is equal to the mean intensity over said volume and angle [39,43]. In the facial area summation, I_i^l represents radiative intensity in direction $\hat{\boldsymbol{s}}^{\boldsymbol{l}}$ at control-volume face i, A_i is the facial surface area, and D_i^l is the directional weight (an analog of the DOM weighting factor), evaluated as:

$$D_i^l = \int_{\Delta\Omega^l} (\hat{\boldsymbol{s}}^{\boldsymbol{l}}\cdot\hat{\boldsymbol{n}}_{\boldsymbol{i}})\, d\Omega^l \tag{4}$$

where the unit vector $\hat{\boldsymbol{n}}_{\boldsymbol{i}}$ is normal to control-volume surface i.

In the radiative source term of Eq. (3b), $\overline{\Phi}^{l'l}$ is the average scattering phase-function between two discrete solid angles $\Delta\Omega^{l'}$and $\Delta\Omega^l$, which can be approximated as follows [40]:

$$\overline{\Phi}^{l'l} \cong \frac{1}{\Delta\Omega^{l'}\Delta\Omega^l}\sum_{l_s=1}^{M_s}\sum_{l_s'=1}^{M_s'}\Phi^{l_s'l_s}\Delta\Omega^{l_s'}\Delta\Omega^{l_s} \tag{5}$$

where the solid angles $\Delta\Omega^{l'}$and $\Delta\Omega^l$ have been divided into numerous sub-angles $\Delta\Omega^{l_s'}$ and $\Delta\Omega^{l_s}$. In Eq. (5), $\Phi^{l_s'l_s}$ is the discrete scattering phase function between sub-angles $\Delta\Omega^{l_s'}$ and $\Delta\Omega^{l_s}$, and M_s and M_s' are the total number of sub-angles used to divided solid angles $\Delta\Omega^{l'}$and $\Delta\Omega^l$. The importance of this phase-function splitting technique will be discussed in more detail shortly.

Unlike the DOM, where the chosen quadrature must satisfy directional moment conditions, the choice of discrete directions for the FVM is generally arbitrary and flexible. One of the more common FVM discretization methods is to divide the total solid angle of 4π into $M = (N_\phi \text{ x } N_\theta)$ equally spaced discrete directions, where N_θ and N_ϕ are the number of divisions in the polar and azimuthal angles, respectively. This angular discretization can result in highly non-uniform solid angles for 3-D problems [70]. As a means of correcting this issue, Kim and Huh [70] introduced the FT_N-FVM angular discretization, where M = N(N+2). This quadrature scheme was shown to eliminate strong non-uniformities in the discrete solid angles, in addition to producing radiative transfer results that are of equal or better accuracy to the equally spaced quadrature. Thus, the FT_N-FVM discretization is applied for all FVM results generated in this study.

Additional details on the discretization of the ERT and FVM solution procedure are not presented here, for brevity, but are available in references [39,40,45].

PHASE-FUNCTION NORMALIZATION FOR DIFFUSE RADIATION

Phase Functions

Radiation scattering by spheres described by the Mie phase function Φ is generally highly oscillatory in nature, and can be expressed as an infinite series of Legendre polynomials, as follows:

$$\Phi(\Theta) = 1 + \sum_{i=1}^{\infty} C_i P_i(\cos\Theta) \tag{6}$$

where Θ is the scattering angle between incoming and outgoing radiation directions, and the coefficients C_i are determined via Mie theory. The oscillatory behavior of the Mie phase function makes it difficult to implement numerically. To this end, it is common to approximate Φ through truncation of the Legendre series to a finite number of terms, as follows:

$$\Phi_{\mathrm{L}}(\Theta) = 1 + \sum_{i=1}^{N} C_i P_i(\cos\Theta) \tag{7}$$

where N is the chosen term of approximation.

Another commonly implemented phase function approximation, due to its ability to accurately represent the strong forward scattering peak in anisotropic scattering such as in biological tissues, is the Henyey-Greenstein (HG) phase-function, whose analytical form is:

$$\Phi_{\mathrm{HG}}(\Theta) = \frac{1-g^2}{[1+g^2-2g\cos\Theta]^{1.5}} \tag{8}$$

where the phase-function asymmetry factor g represents the average cosine of scattering angle, which relates to the Mie coefficient C_1 as $g = C_1/3$. Examples of some typical Legendre polynomial phase-functions are presented in Figure

1a. The Mie coefficients for the seven Legendre polynomials in Figure 1a are presented by Lee and Buckius [71] and Kim and Lee [72]. In Figure 1b, five typical HG phase-functions with varying asymmetry factor are presented.

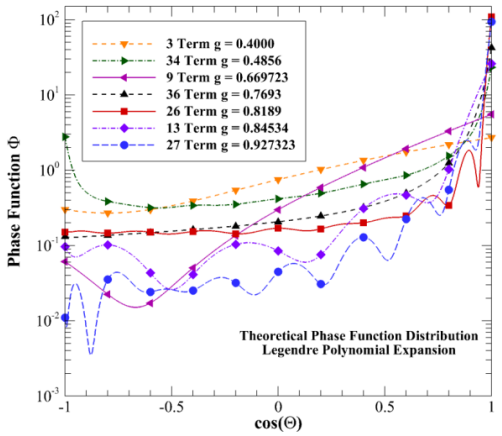

(a)

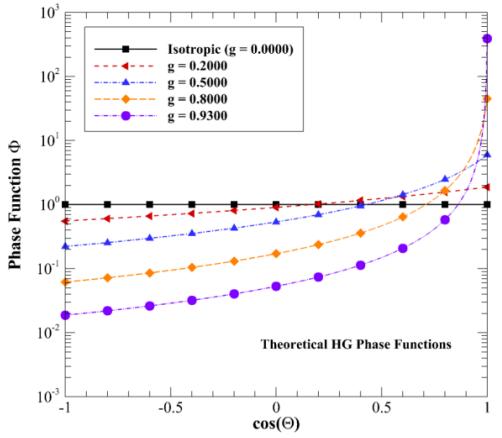

(b)

Figure 1: a) Legendre and b) HG phase-functions

Conservation of Scattered Energy

When numerical methods are implemented to determine radiative transfer, it is well documented and established that angular discretization must preserve scattered energy conservation in the system. Diffuse scattered energy conservation can be achieved by ensuring that the following relation holds, after directional discretization using the DOM:

$$\frac{1}{4\pi}\sum_{l=1}^{M}\Phi^{l'l}\mathrm{w}^{l}=1\,,\qquad l'=1,2,\ldots,M \tag{9}$$

For isotropic scattering ($\Phi = 0$), this equation is satisfied explicitly. However, for anisotropic scattering, this constraint may not be accurately satisfied after DOM discretization, especially for strong-forward phase-functions [62,63].

To illustrate this phenomenon, Figure 2a examines the conservation of scattered energy (represented by a unity value) versus prescribed HG phase-function asymmetry factor for the DOM S_N quadrature with M = 24, 80, and 168 discrete directions. Scattered energy conservation values are calculated as the left-hand side of Eq. (9), and are plotted for all discrete directions. As seen in the inlay of Figure 2a, scattered energy values start to deviate quickly for the S_4 set, reaching differences of greater than 1% for $g \geq 0.40$. For S_8, deviations manifest slightly less quickly, with differences >1% witnessed for $g \geq 0.45$. As the quadrature increases to S_{12}, differences of >1% are witnessed for $g \geq 0.60$. In general, additional phase-function treatment is required for $g \geq 0.35$, 0.40, and 0.60 for S_4-S_{12}, respectively, in order to ensure accurate conservation of scattered energy in the system.

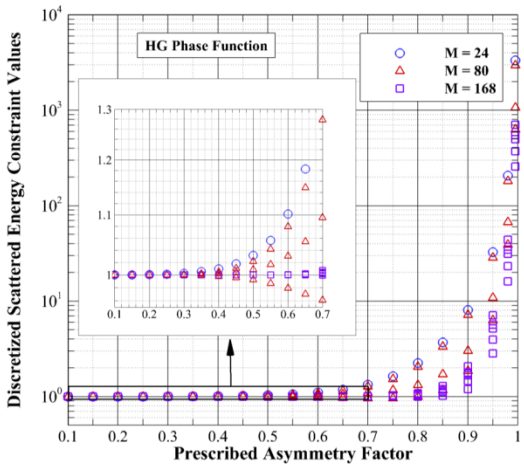

(a)

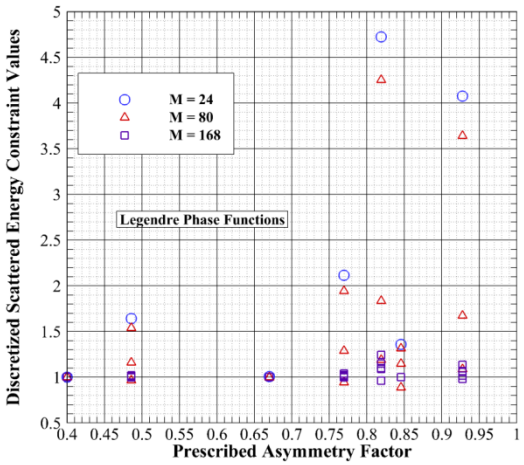

(b)

Figure 2: Examination of conservation of scattered energy vs. prescribed phase-function asymmetry factor using DOM S_4, S_8 and S_{12} quadratures: a) HG phase-function, b) Legendre phase-functions (reproduced from [57])

Figure 2b examines the conservation of scattered energy versus prescribed asymmetry factor for the seven Legendre polynomial phase-functions seen in Figure 1. For the Legendre functions, errors in conservation of scattered energy do not follow the strictly increasing relationship witnessed for the HG

phase function with an increase in g. For example, the maximum deviations for all three quadratures occur for g = 0.8189, reaching 372.5% and 24.6% for S_4 and S_{12}, respectively. This phenomenon stems from both the exact shape of the Legendre phase function, as well as the number of terms in the phase function expansion. The number of terms and magnitude of coefficients of the higher-order terms have a large impact on the exact shape of the phase function. Since asymmetry factor is solely determined by the coefficient C_1, two phase functions with identical asymmetry factors may have significantly different shapes and oscillatory behavior, leading to the nonlinear correlation between scattered energy conservation and asymmetry factor.

The non-conservation of scattered energy after DOM discretization shown in Figures 2a and 2b has been previously shown to result in significant radiative transfer errors. Additionally, for many cases, large scattered energy discrepancies can cause the iterative solution of the ERT to diverge, rendering simulation useless. Thus, to correct this issue, phase-function normalization is commonly implemented. The most common approach to conserve scattered energy is to normalize the phase function using a uniform directional averaging technique, as follows [60]:

$$\tilde{\Phi}^{l'l} = \Phi^{l'l} * \left(\frac{1}{4\pi} \sum_{l=1}^{M} \Phi^{l'l} w^{l} \right)^{-1} \qquad (10)$$

Normalization of the scattering phase function by the inverse of the scattered energy summation will automatically guarantee the accurate conservation of scattered energy after directional discretization. This averaging technique is referred as "scattered energy normalization" in the followings.

Angular False Scattering

In addition to the conservation of scattered energy constraint of Eq. (9), the following constraint must also be satisfied after DOM directional discretization:

$$\frac{1}{4\pi} \sum_{l=1}^{M} \Phi^{l'l} \cos\Theta^{l'l} w^{l} = g\,, \qquad l' = 1,2,\dots,M \qquad (11)$$

Eq. (11) is a constraint on the phase-function asymmetry factor whose satisfaction leads to preservation of the original scattering properties of the prescribed phase function after directional discretization.

Figures 3a and 3b plot discretised phase-function asymmetry factor versus prescribed asymmetry factor for HG and Legendre phase-functions, respectively, generated using the DOM S_4, S_8, and S_{12} quadratures. For all cases, Eq. (10) has been implemented to conserve scattered energy. For the HG phase functions in Figure 3a, discretised asymmetry factor overpredicts the prescribed value by >1% for $g \geq 0.3000$ for the S_4 quadrature, with error reaching 14.8% for g = 0.8000. For the S_8 quadrature, differences of 1% are not reached until g = 0.7000. For the S_{12} quadrature, a difference of 4.2% is seen for g = 0.9000. For the Legendre phase functions presented in Figure 3b, asymmetry factor is effectively conserved for all DOM quadrature sets for g = 0.4000, and within 1.3% for all quadratures with g = 0.6697. The largest differences in discretized asymmetry factor for S_8 and S_{12} occur for g = 0.8189 (matching to the largest discrepancies in scattered energy conservation seen in Figure 2b), reaching 6.9% and 2.6%, respectively. Clearly, phase-function asymmetry factor is not accurately conserved after discretization, even with application of scattered energy normalization.

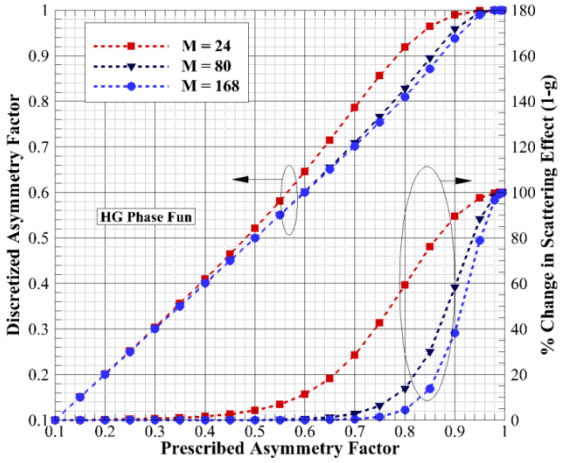

(a)

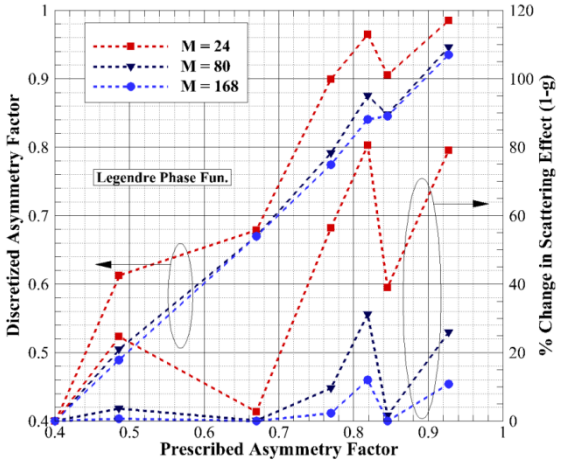

(b)

Figure 3: Comparison of discretized and prescribed asymmetry factor and change in scattering effect after application of scattered energy normalization for a) HG phase-functions and b) Legendre phase-functions

While differences of these magnitudes may not seem critical, it is important to notice that the overall change in scattering effect due to alteration of phase-function asymmetry factor is manifested in the difference in (1-g), according to the isotropic scaling law [71-74]. To this end, the percentage change in (1-g) after discretization is also presented in Figures 3a and 3b. Differences in scattering effect of >20% in Fig. 3a

are encountered for g > 0.6500, 0.8000, and 0.8500 for the three quadratures, respectively. As prescribed asymmetry factor increases further, scattering effect change becomes extremely large, reaching between 75-100% for all three quadratures at the prescribed g = 0.9500.

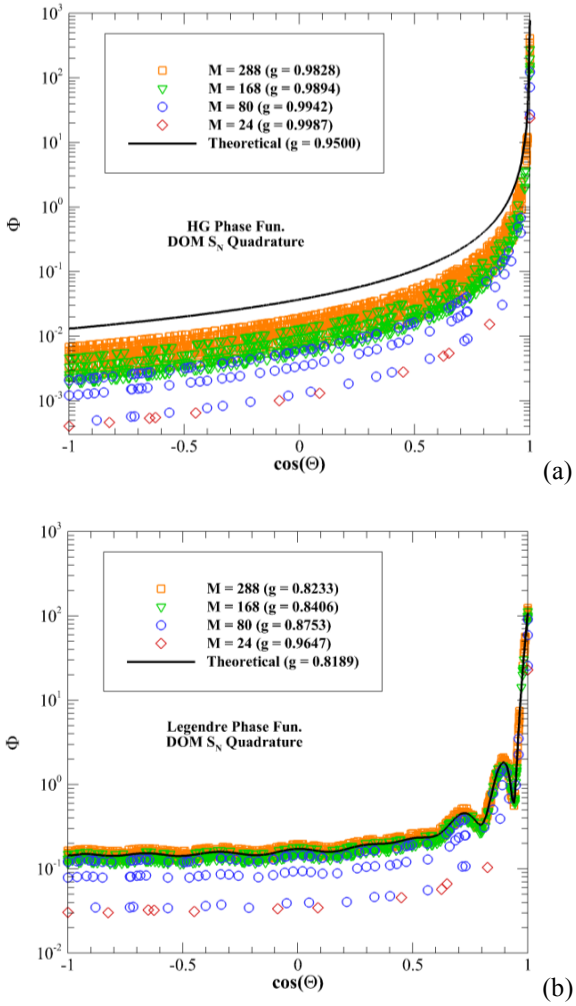

Figure 4: Discretized phase-function values for a) HG g = 0.9500 and b) Legendre g = 0.8189

Additional visualization of the lack of asymmetry factor conservation after application of scattered energy normalization can be seen in Figures 4a and 4b, where plot discretized phase-function values, generated using the DOM S_4, S_8, S_{12}, and S_{16} quadratures, against the theoretical values, for prescribed HG g = 0.9500 and Legendre g = 0.8189 phase functions, respectively. Use of scattered energy normalization greatly alters the shape of the discretized phase-functions, as well as the asymmetry factor values (for g = 0.9500 to discretized values of g = 0.9987, 0.9942, 0.9894, and 0.9828 for the four quadratures, respectively; and for g = 0.8189 to discretized values of g = 0.9647, 0.8753, 0.8406, and 0.8233).

Alteration of phase-function asymmetry factor due to angular discretization can dramatically change the scattering properties of the medium, leading to errors in radiative transfer predictions. We named this type of numerical error as "**angular false scattering**".

The spatial discretization error commonly known as false scattering is an analog to artificial diffusion/numerical smearing in CFD problems [54]. As referenced [50], errors of this type were termed "false scattering" because these errors appear to emulate unrealistic and nonphysical scattering behavior. However, calling such errors by the name "false scattering" is, in essence, a ***misnomer***, as they depend solely on spatial discretization, and are not impacted in any way by angular discretization or the scattering phase function. In the authors' opinion, angular false scattering errors are the true "false scattering" errors, as they result from a direct alteration of scattering behavior in the medium. Thus, it is more appropriate to refer to spatial discretization errors as "numerical smearing", while reserving "false scattering" for errors resulting from the concepts presented in Figures 3 and 4. However, as the use of the term "false scattering" has become widespread in the field, the true false scattering errors will henceforth be referred to as "angular false scattering", as to limit confusion.

As a means of visualizing the impact of angular false scattering errors, radiative transfer in a benchmark test problem is analysed. The test problem involves radiative transfer in a cubic enclosure of edge length L housing an absorbing-emitting and anisotropically scattering medium. The participating medium is taken to be cold (I_b = 0), and all walls except z^* = 0 are taken as cold and black. The wall at z^* = 0 is taken to be a diffuse blackbody emitter, with unity emissive power. The optical thickness is defined as $\tau = (\sigma_a + \sigma_s)L$, and the scattering albedo is $\omega = \sigma_s/(\sigma_a + \sigma_s)$. Unless otherwise mentioned, the staggered spatial grid is taken as $(N_x \text{ x } N_y \text{ x } N_z)$ = (27 x 27 x 27) in all simulations. The spatial coordinates are non-dimensionalized by the edge length, as follows: $x^* = x/L$, $y^* = y/L$, and $z^* = z/L$. The positive differencing scheme is implemented for all DOM simulations. All radiative transfer computations are performed in the FORTRAN computing language on a Dell Optiplex 780 workstation, with an Intel Core 2 processor and 4.0 GB of RAM.

A comparison of heat fluxes generated using the DOM S_{12} quadrature with scattered energy normalization are compared to published Monte Carlo (MC) results [53] to gauge their accuracy in Figure 5. Heat fluxes are calculated at the centerline of the wall directly opposite from the diffuse source, i.e. $Q(x^*, y^* = 0.5, z^* = 1.0)$. The optical thickness and scattering albedo of the medium are taken as τ = 10.0 and ω = 1.0, while solutions are determined using the HG phase-function approximation with g = 0.2000, 0.8000, and 0.9300, respectively.

For weak-forward scattering (g = 0.2000), DOM predictions conform accurately to the MC prediction, with differences of between 1-5% occurring. Differences of these magnitudes are reasonable between MC and DOM, due to both DOM numerical errors and MC statistical errors. Additionally, as seen in Figure 3a, asymmetry factor is not significantly altered after DOM discretization for g = 0.2000, so accurate

conformity between DOM and MC is expected. As asymmetry factor increases to g = 0.8000, the DOM begins to overpredict the MC solution by between 6-9%, corresponding to the small alteration in discretized asymmetry factor to g = 0.8089. For g = 0.9300, the discretized asymmetry factor is dramatically altered to g = 0.9735, leading to DOM heat fluxes overpredicting MC by over 30%. Errors due to angular false scattering are extremely evident in Figure 5.

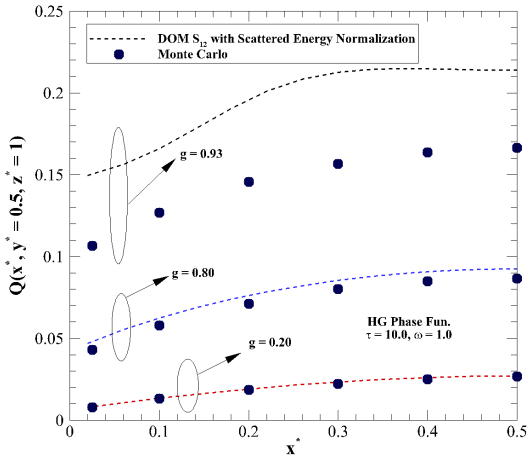

Figure 5: Comparison of Q(x*, y* = 0.5, z* = 1.0) generated using DOM S_{12} with scattered energy normalization vs. Monte Carlo solution [53] for HG g = 0.2000, 0.8000, and 0.9300

As previously discussed, the S_N quadrature has a directional limit, imposed by directional moment constraints. More recently, non-limited quadratures, such as the P_N-T_N Legendre-Chebyshev quadrature of Longoni and Haghighat [64] have been developed. Following the trend witnessed for increasing direction number for scattered energy conservation in Figure 1a and asymmetry factor conservation in Figure 3a, it seems reasonable to assume that, with a fine enough angular resolution, both critical quantities may be able to be conserved without requiring phase-function normalization. To this end, a comparison of non-normalized DOM heat flux $Q(x^*, y^* = 0.5, z^* = 1.0)$ generated using the P_N-T_N quadrature with extremely high discrete direction numbers with benchmark MC results is presented in Figure 6 for HG g = 0.93. DOM heat flux profiles are generated using indices N = 44, 52, and 64, corresponding to discrete direction number M= 2024, 2808, and 4224, respectively.

The three non-normalized profiles show a converging trend as discrete direction number increases. For M = 2024, differences of between 27-30% exist when compared to MC, corresponding to a distortion of g to 0.9453. While scattered energy is conserved well enough in this case to allow for a converged solution, the angular grid is still too coarse to obtain accurate solutions. Increases in direction number to 2808 reduces errors with respect to MC to <10% (discretized g = 0.9356), while use of the extreme M = 4224 quadrature results in MC and DOM errors conforming to each other within 1.5%. This solution corresponds to discretized g = 0.9313. As an additional comparison, applying scattered energy normalization to this quadrature reduces the discretized g to 0.9301, resulting in heat fluxes that underpredict MC by less than 2.5% at all locations.

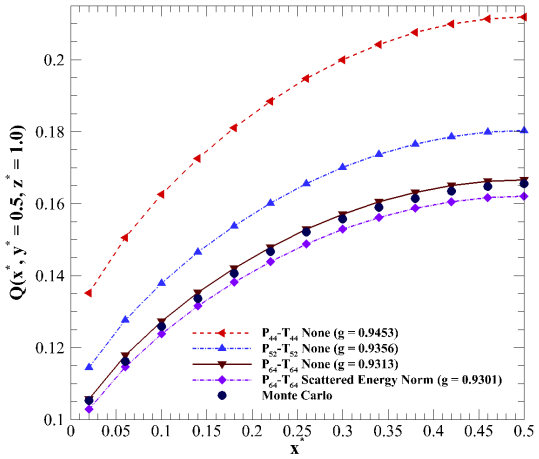

Figure 6: Comparison of Q(x*, y* = 0.5, z* = 1.0) generated using DOM without normalization for extremely high discrete direction numbers (reproduced from [58])

While Figure 6 shows that higher-order DOM quadrature sets have the advantage of minimizing angular false scattering error, a major disadvantage of this approach lies in computational efficiency, as increases in discrete direction number directly result in both higher computational convergence time and memory requirements. For the S_{16} quadrature (M = 288), the computational convergence time for this benchmark problem is ~13 minutes. As discrete direction number increases, computational time increases in a non-linear fashion, with increases in discrete direction number to 2024 and 4224 requiring 1330 and 7107 minutes (4.94 days) to converge. These extremely high convergence times illustrate the impracticality of using higher-order quadratures to obtain accurate radiative transfer solutions.

The preceding results indicate major issues with the use of the commonly implemented scattered energy normalization approach of Eq. (10). While minimization/elimination of angular false scattering is possible through use of extreme quadrature, efficiency suffers greatly. In order to limit computational resources to a reasonable amount and maintain radiative transfer accuracy by limiting angular false scattering, additional normalization techniques should be explored.

Mishchenko et al.'s Scattered Energy Normalization

More recently, Mishchenko et al. [75] introduced an additional normalization technique, specifically crafted to accurately conserve scattered energy. Rather than modifying all discrete phase function values in the system, they wisely noted that, for the strong-forward scattering HG phase function, the magnitude of the forward-scattering term $\Phi^{l'l'}$ is significantly larger than the remaining discrete phase function values. Thus, they proposed to conserve scattered energy

solely through normalization of the forward-scattering phase-function term, leaving all other values of $\Phi^{l'l}$ unaltered.

Applying this notion, the normalized value of the forward-scattering phase-function term can be expressed as follows:

$$\tilde{\Phi}^{l'l'} = \left(1 + A^{l'}\right)\Phi^{l'l'} \tag{12}$$

where $A^{l'}$ is the forward-scattering normalization vector parameter. Using Eq. (12) to normalize the forward-scattering term, the scattered energy condition of Eq. (9) can be rewritten in the following manner, for discrete direction $\hat{\boldsymbol{s}}^{\boldsymbol{l'}}$:

$$\frac{1}{4\pi}\sum_{\substack{l=1 \\ l'\neq l}}^{M} \Phi^{l'l} w^{l} + \frac{1}{4\pi}\left(1 + A^{l'}\right)\Phi^{l'l'} w^{l'} = 1 \tag{13}$$

Solving for $A^{l'}$ leads to the following expression for the forward-scattering normalization vector parameter for a given discrete direction $\hat{\boldsymbol{s}}^{\boldsymbol{l'}}$:

$$A^{l'} = \left(4\pi - \sum_{l=1}^{M} \Phi^{l'l} w^{l}\right) / \left(\Phi^{l'l'} w^{l'}\right) \tag{14}$$

While this normalization approach does guarantee accurate conservation of scattered energy in a simpler manner than the traditional formulation of Eq. (10), it does not mathematically guarantee accurate conservation of asymmetry factor, and thus will suffer from angular false-scattering. For future reference, Eqs. (12-14) will be referred to as "Mishchenko's E" normalization.

Kamdem Tagne's Asymmetry Factor Normalization

Recently, Kamdem Tagne [76] extended the formulation of Mishchenko et al. to develop a normalization technique that guarantees preservation of asymmetry factor after discretization. As with Mishchenko's E normalization, only the forward-scattering term is normalized. However, instead of using Eq. (9) as the basis for determining the normalization parameters, as presented in the previous section, the asymmetry factor conservation condition of Eq. (11) is used. Using Eq. (12) in conjunction with Eq. (11), the forward-scattering normalization parameters that will accurately conserve asymmetry factor after discretization become:

$$A^{l'} = \left(4\pi g - \sum_{l=1}^{M} \Phi^{l'l} \cos\Theta^{l'l} w^{l}\right) / \left(\Phi^{l'l'} w^{l'}\right) \tag{15}$$

This technique will not experience angular false scattering errors, as g is always conserved, but mathematically accurate conservation of scattered energy is not guaranteed, a fact that could lead to significant discrepancies in radiative transfer predictions. For future reference, the normalization of Eqs. (12) and (15) will be referred to as "Kamdem Tagne's g" normalization.

Table 1 addresses the lack of either scattered energy or asymmetry factor conservation after application of scattered energy, Mishchenko's E, and Kamdem Tagne's g normalizations. Scattered energy and asymmetry factor values are tabulated for P_N-T_N quadrature indices of N = 4, 6, 8, 12, and 16, corresponding to M = 24, 48, 80, 168, and 288, respectively. Three typical values of HG asymmetry factor are presented: g = 0.6000, 0.8000, and 0.9300. As additional means of comparison, values calculated without normalization are presented. Percent differences in scattered energy E and in scattering effect (1-g) are also listed, in order to gauge the significance of lack of quantities conservation.

Table 1: Discretized scattered energy and/or asymmetry factor values for various normalization techniques using DOM P_N-T_N quadrature and HG phase function with g = 0.6000, 0.8000, and 0.9300

		No Normalization		Scattered Energy Norm.		Mishchenko E		Kamdem Tagne g	
g	N	Discretized E	Discretized g	Discretized g	% Diff in (1-g)	Discretized g	% Diff in (1-g)	Discretized E	% Diff in E
0.6000	4	1.0741	0.6818	0.6347	8.684	0.6077	1.917	0.9923	0.7669
	6	1.0111	0.6123	0.6056	1.399	0.6012	0.308	0.9988	0.1231
	8	1.0018	0.6021	0.6009	0.237	0.6002	0.053	0.9998	0.0213
	12	1.0001	0.6001	0.6000	0.009	0.6000	0.002	1.0000	0.0008
	16	1.0000	0.6000	0.6000	0.000	0.6000	0.000	1.0000	0.0000
0.8000	4	2.2171	2.0349	0.9177	58.87	0.8177	8.868	0.9823	1.7737
	6	1.4274	1.2346	0.8648	32.38	0.8072	3.604	0.9928	0.7209
	8	1.1695	0.9726	0.8315	15.77	0.8031	1.555	0.9969	0.3110
	12	1.0312	0.8318	0.8066	3.322	0.8006	0.314	0.9994	0.0628
	16	1.0064	0.8065	0.8014	0.703	0.8001	0.068	0.9999	0.0135
0.9300	4	16.524	16.466	0.9965	94.98	0.9414	16.29	0.9886	1.1400
	6	8.3776	8.3149	0.9925	89.26	0.9373	10.43	0.9927	0.7300
	8	5.1532	5.0880	0.9873	81.82	0.9348	6.857	0.9952	0.4800
	12	2.6833	2.6157	0.9746	63.78	0.9324	3.429	0.9976	0.2400
	16	1.8047	1.7360	0.9617	45.36	0.9313	1.857	0.9987	0.1300

Both scattered energy directional averaging and Mishchenko's E normalizations are able to accurately conserve scattered energy. However, the fact that nearly all phase-function values are preserved using Mishchenko's E normalization leads to much smaller errors in discretized asymmetry factor. Differences in scattering effect change are dramatically reduced when only the forward-scattering term is normalized. However, for strong-forward scattering (g = 0.9300), >5% changes in scattering effect are observed for N <12, indicating the potential for potentially crucial angular false scattering errors.

As seen in Table 1, while Kamdem Tagne's g normalization does conserve asymmetry factor (thus minimizing angular false scattering), conservation of scattered energy is not guaranteed after directional discretization. Discrepancies in scattered energy increase as asymmetry factor increases, although the values remain <1% for all quadratures except N = 4. Although deviations in scattered energy are not of high magnitude, accumulation of errors during computation due to lack of energy conservation can be appreciable and/or lead to divergence of the iterative solution.

Hunter and Guo's 2012 Normalization

The results presented in Figures 5-6 indicate the importance of conserving both scattered energy and phase-function asymmetry factor after directional discretization, in order to limit numerical error due to angular false scattering. To improve radiative transfer prediction accuracy and efficiency, a phase-function normalization technique that ensures the numerically accurate conservation of Eqs. (9) and (11) after discretization of the continuous angular variation of radiation scattering is desired.

To this end, Hunter and Guo [55] proposed that the scattering phase function $\Phi^{l'l}$ be normalized in the following manner, for all discrete radiation directions $\hat{\boldsymbol{s}}^{\boldsymbol{l}}$:

$$\tilde{\Phi}^{l'l} = \left(1 + A^{l'l}\right)\Phi^{l'l} \tag{16}$$

where the normalization parameters $A^{l'l}$ correspond to radiation scattering between two discrete radiation directions $\hat{\boldsymbol{s}}^{\boldsymbol{l'}}$ and $\hat{\boldsymbol{s}}^{\boldsymbol{l}}$. The normalized scattering phase-function $\tilde{\Phi}^{l'l}$ satisfies three conditions: the scattered energy constraint of Eq. (9), the asymmetry factor constraint of Eq. (11), and a directional symmetry constraint (i.e., $\tilde{\Phi}^{l'l} = \tilde{\Phi}^{ll'}$).

The system comprised of Eq. (16) and Eqs. (9), (11), and the directional symmetry constraint is underdetermined, as there are $M(M+1)/2$ unknown normalization parameters $A^{l'l}$ and only $2M$ equations (M scattered energy, M asymmetry factor constraints). This system has infinitely many solutions, although only one solution will have the smallest residual error. This solution is known as the "minimum norm" solution, and can be determined using QR factorization or least-squares. The minimum norm solution to the system will generate the normalization parameters $A^{l'l}$ that allow for accurate conservation of scattered energy and asymmetry factor after directional discretization. This normalization technique is formally published in 2012, and thus will be referred to henceforth as "Hunter and Guo's 2012" normalization.

A visualization of the ability of Hunter and Guo's 2012 normalization to preserve asymmetry factor can be seen in Figure 7, in which discretized HG phase-function values are plotted for g = 0.9500 after application of normalization. For all discrete direction numbers, g is accurately conserved after directional discretization, and the discretized values conform closely to the theoretical phase-function shape. Similar results are witnessed for Legendre phase-functions. The improvement in discretized phase-function values over those seen in Figure 4 gives a preliminary indication of reduction in angular false scattering errors.

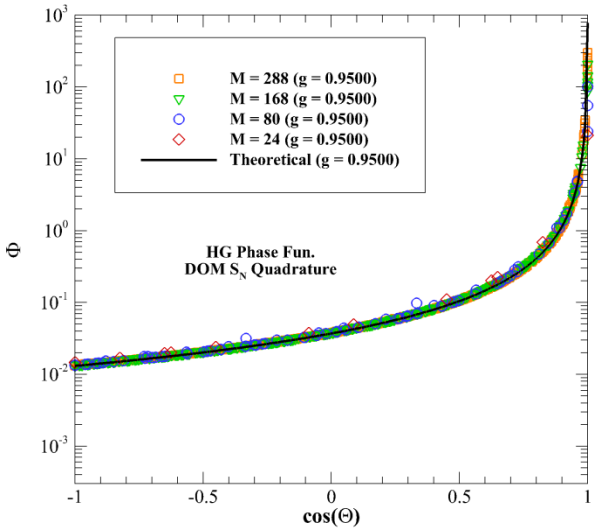

Figure 7: Discretized HG phase-function values after application of Hunter and Guo's 2012 normalization

Hunter and Guo's 2014 Normalization

Both Mishchenko's E and Kamdem Tagne's g normalizations have the inherent advantage of being simple to implement, although each is only able to accurately conserve one of the two quantities of interest. Ideally, these two normalizations could be combined in some way, in order to take advantage of mathematical simplicity whilst retaining conservation of both scattered energy and asymmetry factor.

To this end, Hunter and Guo [59] proposed another normalization technique that normalizes both the forward-scattering term as well as the backward scattering term $\Phi^{l'l^-}$, where the superscript l^- represents the radiation direction directly opposite from $\hat{\boldsymbol{s}}^{\boldsymbol{l'}}$, with $\cos\Theta^{l'l^-} = -1$. Applying this idea, the normalized values of the forward and backward scattering phase function terms can be expressed as follows:

$$\tilde{\Phi}^{l'l'} = \left(1 + A^{l'}\right)\Phi^{l'l'} \tag{17a}$$

$$\tilde{\Phi}^{l'l-} = \left(1 + B^{l'-}\right)\Phi^{l'l-} \tag{17b}$$

where $B^{l'-}$ is the backward-scattering normalization vector parameter. Simultaneous solution of Eqs. (9) and (11) after substitution of Eqs. (17a-b) leads to the following expressions for the forward-and backward-scattering normalization parameters:

$$A^{l'} = \frac{1}{2\Phi^{l'l'}w^{l'}}\left[4\pi(1+g) - \sum_{l=1}^{M}\Phi^{l'l}w^{l}\left(1+\cos\Theta^{l'l}\right)\right] \tag{18a}$$

$$B^{l'-} = \frac{1}{2\Phi^{l'l-}w^{l-}}\left[4\pi(1-g) + \sum_{l=1}^{M}\Phi^{l'l}w^{l}\left(\cos\Theta^{l'l}-1\right)\right] \tag{18b}$$

Use of these normalization parameters will guarantee conversion of both scattered energy and asymmetry factor simultaneously, as Hunter and Guo's 2012 normalization also does. For future reference, this normalization will be referred to as "Hunter and Guo's 2014" normalization since it is formally published in 2014.

Comparison of Normalizations

In all five afore-discussed normalizations the forward-scattering phase function term is normalized in some fashion, in order to artificially reduce the forward-scattering peak. Figure 8 plots the values of the forward-scattering normalization parameters for the DOM P_8-T_8 quadrature (M = 80) for the five normalizations using a prescribed HG asymmetry factor of g = 0.9300. The parameters are presented only for directions located in the principal octant, due to DOM symmetry. For Hunter and Guo's 2012 normalization, the normalization parameters $A^{l'l'}$ are shown, while Mishchenko's E, Kamdem Tagne's g, and Hunter and Guo's 2014 normalizations, the forward-scattering normalization parameter $A^{l'}$ are presented. For scattered energy normalization, the value presented is the value of the inverse summation in Eq. (10) minus one.

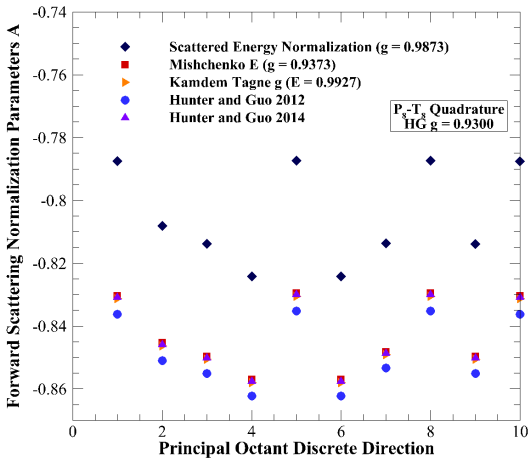

Figure 8: Comparison of forward-scattering normalization parameters in the principal octant among various normalization techniques using the P_8-T_8 quadrature (M = 80 discrete directions) (reproduced from [59])

As seen in Figure 8, the parameters generated with the three normalizations that solely normalize the forward-scattering term are nearly identical for all directions, indicating that these three normalizations are all similarly attenuating the forward-scattering term. However, slight differences in forward-scattering parameter lead to nonconservation of scattered energy in Kamdem Tagne's g normalization, and nonconservation of asymmetry factor in Mishchenko's E normalization.

The forward-scattering parameters calculated using Hunter and Guo's 2012 normalization are slightly lower in magnitude than the three previously discussed normalizations, due to the fact that drops in forward-scattering phase-function term are counteracted by slight increases in the remaining phase-function values in the system. It is important to mention that all parameters are >-1, meaning that normalized phase-function values remain positive after application of normalization. For scattered energy normalization, while at first glance the forward-scattering peak is more accurately represented after discretization, the massive shift in the remaining phase-function values due to alteration of g, and the resultant angular false scattering errors, make this normalization less than desirable. From this point further, for the DOM, results for the scattered energy normalization of Eq. (10) will no longer be presented.

In Hunter and Guo's 2014 normalization, the backward-scattering phase-function terms are normalized. For the HG phase-function, the backward-scattering parameters tend to attain high positive values (of up to 40), which greatly increase the value of the phase-function at this point [59]. The impact of such high positive backward-scattering parameters is seen in Figure 9, in which discretized values of the normalized backward-scattering phase-function term are plotted against the theoretical values.

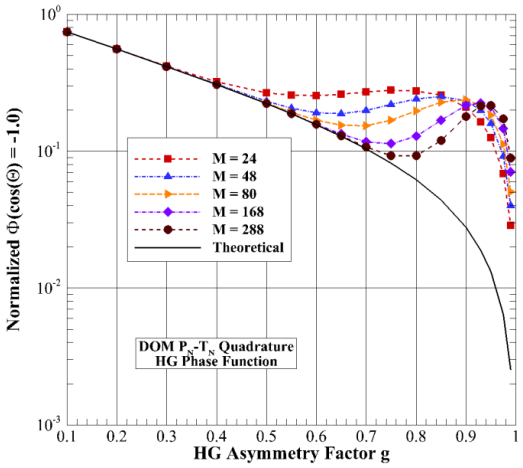

Figure 9: Normalized backward-scattering discrete phase-function values for various discrete direction numbers versus HG asymmetry factor (reproduced from [59])

The results in Figure 9 show that parameter values on the order of ~10-40 correspond to minor increases in terms of absolute value change in phase-function. At g = 0.9300, the

backward-scattering phase-function value theoretically should be 0.019. After application of Hunter and Guo's 2014 normalization, this value is increased to 0.179, 0.228, 0.263, 0.301, and 0.309 for M = 24, 48, 80, 168, and 288, respectively. While these differences are relatively large, the increased phase-function values are still significantly smaller in magnitude than the forward-scattering peak value for highly-anisotropic scattering. Further, the values are still significantly less than unity, meaning that the impact of such high backward parameters will not be of major concern.

Figures 10a and 10b compare DOM heat fluxes $Q(x^*, y^* = 0.5, z^* = 1.0)$ generated using Mishchenko's E, Kamdem Tagne's g, Hunter and Guo's 2012, and Hunter and Guo's 2014 normalizations. In both figures, the DOM P_N-T_N quadrature is used, the medium optical thickness and scattering albedo are τ = 10.0 and ω = 1.0, respectively, and the HG asymmetry factor is g = 0.9300. Benchmark MC results, as well as FVM heat fluxes generated with an extremely high direction number (M = 2400), are plotted for comparison.

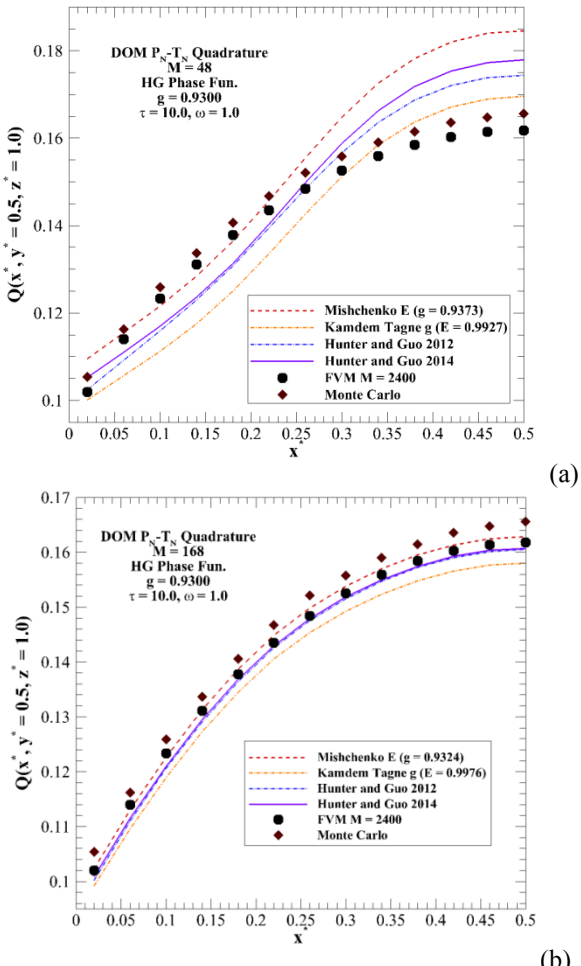

Figure 10: Comparison of Q(x^*, y^* = 0.5, z^* = 1) between DOM solutions generated with various phase-function normalizations and FVM and Monte Carlo predictions using g = 0.9300 with a) M = 48 and b) M = 168 (reproduced from [59])

In Figure 10a (M = 48), heat fluxes generated using Mishchenko's E normalization overpredict Hunter and Guo's 2014 normalization by ~4%, corresponding to discretized g = 0.9373. An overprediction in heat flux is consistent with a higher discretized asymmetry factor, as radiant energy more strongly propagates through the medium towards the wall of interest. Conversely, application of Kamdem Tagne's g normalization results in a heat flux underprediction of about 5% as compared to Hunter and Guo's 2014 normalization, corresponding to the underconservation of scattered energy (E = 0.9886). When comparing Hunter and Guo's 2014 normalization to Hunter and Guo's 2012 normalization, maximum and average errors of 2.5% and 1.4%, respectively, are encountered. Accurate conformity of these two normalizations is expected, as they both conserve scattered energy and asymmetry factor. For this low directional order, DOM heat fluxes suffer greatly from ray effect error, leading to the significant change in heat flux shape when compared with FVM and MC. It is notable that the FVM and MC heat fluxes differ by between 2-3%, which is an acceptable error due to FVM approximation and MC statistical errors.

When discrete direction number is increased to M = 168 in Figure 10b, an overall reduction in the discrepancies in asymmetry factor and energy conservation for Mishchenko's E and Kamdem Tagne's g normalizations is witnessed. Heat flux generated with Mishchenko's E normalization (g = 0.9324) overpredicts Hunter and Guo's 2014 normalization by 1.3% on average, while Kamdem Tagne's g normalization underpredicts by 1.7% on average (E = 0.9976). More importantly, the profiles generated using both of Hunter and Guo's normalizations are nearly identical, while also conforming to within 1% on average to the FVM with M = 2400. This gives extreme confidence that Hunter and Guo's 2012 and 2014 normalizations are able to produce accurate radiative transfer predictions. Additionally, use of the DOM with normalization presents a distinct advantage in computational efficiency over the high-order FVM. For M = 168, DOM using Hunter and Guo's 2014 normalization converges in 5.53 minutes, while the FVM with 2400 discrete directions requires 37.25 hours. Use of proper normalization in conjunction with the DOM reduces computational time by 99.8% while retaining solution accuracy.

For the medium analyzed in Figures 5, 6, and 10, the reduced optical thickness $(1-g)\tau$ is 0.7. For many turbid media, such as biological tissues, it is common for the reduced optical thickness to be >>1. To this end, Figure 11 presents an analysis of the impact of normalization on radiative transfer in an optically-thick medium (τ = 100.0) with g = 0.9300 ($(1-g)\tau$ = 7.0). As a means of comparison, FVM heat flux generated with M = 840 discrete directions is also presented. In Figure 11, heat fluxes generated with Mishchenko's E normalization overpredict Hunter and Guo's 2014 normalization, while profiles generated using Kamdem Tagne's g normalization underpredict, similar to the behaviors witnessed in Figure 10. However, the large increase in optical thickness has increased the total number of scattering events, and thus discrepancies in scattered energy and asymmetry factor have a much larger impact on radiative transfer predictions. As compared with the FVM, Mishchenko's E

normalization overpredicts by an average of 12.6% and 4.3% for M = 48 and 288, respectively. Conversely, deviations in scattered energy conservation in Kamdem Tagne's g normalization result in drastic underpredictions of 72.0% and 22.3%, indicating the criticality of scattered energy conservation and the impracticality of Kamdem Tagne's g normalization for optically thick, highly anisotropically-scattering media.

Heat fluxes generated using Hunter and Guo's 2014 normalization conform accurately to within 1% of Hunter and Guo's 2012 normalization, and to within 2.5% of the higher-direction FVM for all quadratures tested. Additionally, the average difference between Hunter and Guo's 2014 normalization for M = 48 and 288 is only 0.70%, indicating that the optically thick medium has mitigated ray effect, and that accurate heat fluxes can be achieved with a coarser angular resolution.

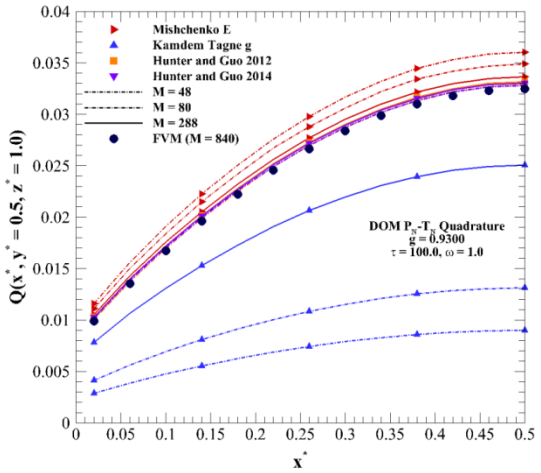

Figure 11: Comparison of Q(x*, y* = 0.5, z* = 1) between DOM solutions with various phase-function normalizations and FVM predictions using g = 0.9300 with M = 48, 80, and 288 discrete directions in an optically thick medium (τ = 100.0) (reproduced from [59])

For the HG phase function, both Hunter and Guo's 2012 and 2014 normalizations conform accurately to FVM, due to the fact that scattered energy and asymmetry factor are accurately conserved. DOM heat fluxes for which the phase-function normalization conserves both E and g simultaneously always lie between the predictions of either conservation alone. Hunter and Guo's 2014 normalization offers an added simplicity of implementation, as it does not require solution of a system of equations. The mathematical advantage of Hunter and Guo's 2014 normalization makes it a desirable technique for accurately determining radiative transfer in a highly-anisotropically scattering media when the HG phase-function approximation is implemented.

While the HG phase-function is a good approximation for strong-forward scattering, it is of interest to compare the normalization approaches for more general Legendre polynomial phase-functions, as they better represent the oscillatory nature of Mie scattering. When the three mathematically simpler normalizations (Mishchenko's E, Kamdem Tagne's g, and Hunter and Guo's 2014) were applied to the HG phase functions, corrected values of $\tilde{\Phi}$ remained positive, as normalization parameters never attained values of less than -1. However, for the general Legendre polynomial phase functions, it is found that application of these simple techniques can, in some cases, lead to either forward- or backward-scattering normalization parameters that are less than -1. This, in turn, leads to physically unrealistic negative values of the normalized phase-function.

In Figures 12(a-b), discretized Legendre phase-function values, generated using Mishchenko's E, Kamdem Tagne's g, Hunter and Guo's 2012, and Hunter and Guo's 2014 normalizations, are plotted against the theoretical phase-function values for two cases: the EO_8 quadrature with g = 0.8189, and the EO_{16} quadrature with g = 0.9273.

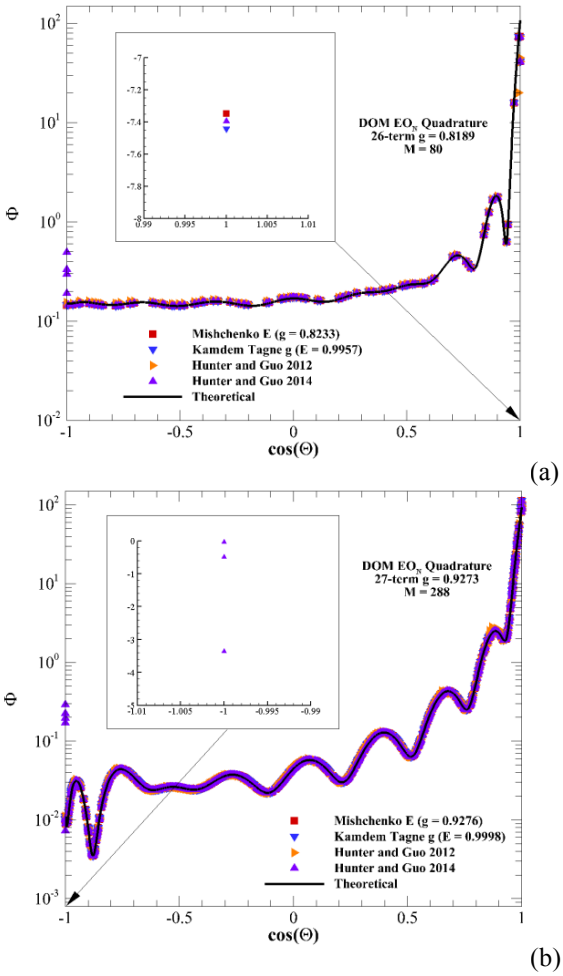

Figure 12: Discretized Legendre phase-function values with a) M = 80 and g = 0.8189, and b) M = 288 and g = 0.9273

In Figure 12a, all four normalizations produce similar phase-function values after discretization at most locations, except at the forward- and backward-scattering directions. At cos Θ = -1, the impact of the backward-scattering normalization parameters is clearly seen for Hunter and Guo's 2014

normalization, as the phase-function values are skewed to much higher values. Of more importance, however, is the behavior at ($\cos\Theta - 1$). The inlay in Figure 12a shows that the three simple normalizations result in some negative phase-function values for the forward direction, indicating that, for Legendre polynomial phase-functions, normalization of solely the forward/backward term(s) might be unsuitable.

In Figure 12b, no negative phase-function values are encountered for the forward-scattering phase function term. However, as seen in the inlay, large difference between the discretized values generated with Hunter and Guo's 2014 normalization and the theoretical are witnessed for $\cos\Theta = -1$, with multiple directions being altered to a negative phase-function value. This error is not present for Mishchenko's E or Kamdem Tagne's g normalization, as they do not involve backward-scattering normalization. Additionally, the negative values for the backward-scattering term are of much lower magnitude than for forward-scattering in Figure 12a.

The minimum values of forward-scattering normalization parameter are plotted in Figure 13, for the principal octant, using the EO_8 quadrature with Legendre g = 0.8189 for the various normalization approaches. Forward parameters for the Mishchenko's E, Kamdem Tagne's g, and Hunter and Guo's 2014 are nearly identical, as witnessed for the HG phase function in Figure 8. For three directions, parameters of <-1 occur, which will result in negative phase-function values. For all but those three directions, Hunter and Guo's 2012 normalization results in very similar forward parameters. However, for those three directions, Hunter and Guo's 2012 normalization does not experience parameters < -1, thus avoiding the critical issue of unrealistically negative phase-function values, and potentially making it the most suitable normalization approach when Legendre polynomial phase functions are implemented..

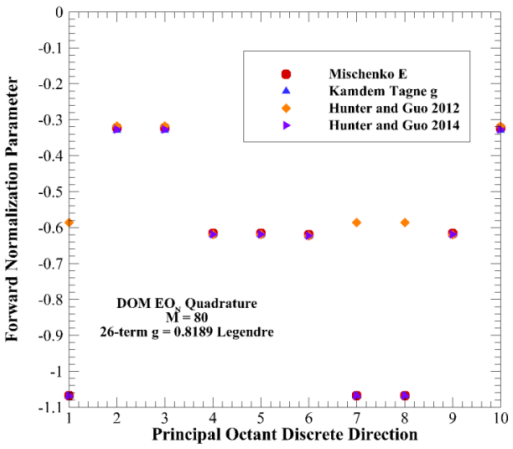

Figure 13: Minimum forward-scattering normalization parameters using various normalization techniques for the DOM EO_N quadrature with M = 80 and g = 0.8189

The appearance of negative phase-function values in three normalization approaches is a potentially critical issue for determination of accurate radiation transfer using the DOM. In order to investigate the impact of negative phase-function values, radiation transfer in the benchmark test problem described previously is investigated in Figures 14-15. During simulation, it was found that negative phase-function values resulted in negative intensity values, regardless of spatial differencing scheme. When negative intensity values occur, the solution of the ERT diverges at the next iteration in the solution procedure, and thus a convergent intensity field cannot be generated. As a means of correcting this issue, the positive scheme [5] for negative intensity correction must be implemented, in which any negative intensities are set to zero immediately after they are encountered in the simulation.

In Figures 14(a-b), non-dimensional heat fluxes are calculated using the DOM with the four normalization techniques previously described. The medium optical thickness is τ = 10.0. Results in Figure 14a are generated using the EO_8 quadrature with Legendre g = 0.8189, while the EO_{16} with Legendre g = 0.9273 is implemented in Figure 14b. As a means of comparison, FVM heat flux profiles generated with the FT_N-FVM quadrature with M = 840 are also plotted.

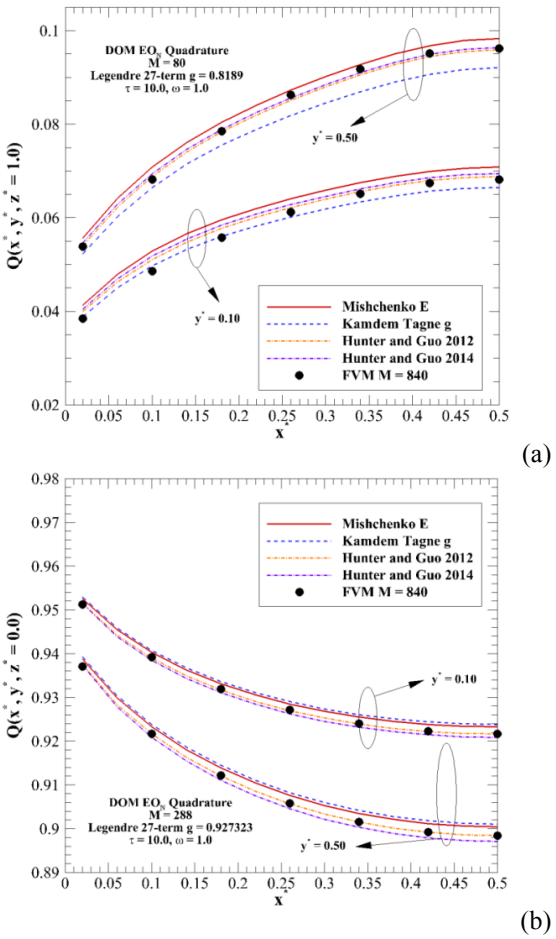

Figure 14: Comparison of heat flux generated with FVM and various DOM diffuse radiation normalization techniques: a) $Q(x^*, y^*, z^* = 1.0)$ with M = 80 and g = 0.8189; b) $Q(x^*, y^*, z^* = 0.0)$ with M = 288 and g = 0.9273

In Figure 14a, negative forward-scattering parameters were encountered for Mishchenko's E, Kamdem Tagne's g, and

Hunter and Guo's 2012 normalizations. These negative forward-parameters lead to the necessity of negative intensity correction. As Hunter and Guo's 2012 normalization does not require such a correction, it is taken as a validation basis for DOM results. Heat fluxes generated with Hunter and Guo's 2014 normalization with negative intensity correction conform accurately within 1.5% to those generated using Hunter and Guo's 2012 normalization. Slight overpredictions of ~3% are witnessed for Mishchenko's E normalization, while slight underpredictions of ~5% are seen for Kamdem Tagne's g normalization, corresponding to lack of asymmetry factor and scattered energy conservation, respectively. When compared to FVM, the four normalizations differ by maximums of 9.0% and 5.5% for $y^* = 0.1$ and 0.5, respectively.

Due to the large absolute values of the backward-scattering normalization parameters inherent in Hunter and Guo's 2014 normalization, it is of interest to examine normalized heat fluxes at the source/hot wall, or $Q(x^*, y^*, z^* = 0)$, in order to determine if a significant change in heat flux flowing back into the hot wall is encountered. From Figure 14b, it is seen that results generated using Hunter and Guo's 2014 normalization conform to Hunter and Guo's 2012 normalization and FVM within 0.2% at all locations, indicating that the large magnitude of backward scattering parameters does not adversely impact radiative transfer predictions at the hot wall.

Finally, Figure 15 presents an analysis of the impact of normalization on heat fluxes at the far wall in an optically thick medium (τ = 100.0) for the EO_{16} quadrature with g = 0.9273. While DOM profiles generated using the other three normalizations conform to FVM within 7% and within 2% to each other, the slight lack of energy conservation inherent in Kamdem Tagne's g normalization results in errors of up to 18%. Analysis of the optically-thick case in Figure 15, as well as in Figure 11 for the HG phase function, indicates the absolute necessity of conserving scattered energy after discretization.

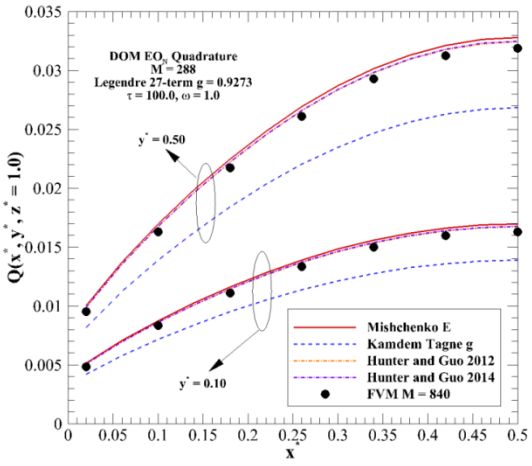

(b)

Figure 15: Comparison of heat flux $Q(x^*, y^*, z^* = 1.0)$ profiles generated with FVM and various DOM diffuse radiation normalization techniques with M = 288 and g = 0.9273 in an optically thick medium

In general, the results show that Hunter and Guo's 2014 normalization may be less useful for Legendre polynomial phase functions than Hunter and Guo's 2012 normalization, due to the fact that negative intensities occur, although radiation transfer predictions appear to be largely unaffected as long as negative intensity correction is implemented. It is recommended that, for HG phase functions, both Hunter and Guo's 2012 and 2014 normalizations can be used. For Legendre polynomial phase functions, Hunter and Guo's 2012 normalization is recommended, as it avoids the necessity of negative intensity correction.

Finite Volume Method

Using the FVM, the scattered energy conservation condition of Eq. (9) can be rewritten in the following manner, implementing the concept of the averaged scattering phase-function:

$$\frac{1}{4\pi}\sum_{l=1}^{M}\bar{\Phi}^{l'l}\Delta\Omega^{l} = 1\,, \qquad l' = 1,2,\ldots,M \tag{19}$$

The use of the averaged scattering phase function, which was first proposed by Chui et al. [40], was suggested as a manner to accurately conserve scattered energy in the system without the necessity of scattered energy normalization. The prevailing theory is that if a fine-enough solid-angle splitting grid is defined, scattered energy will be accurately conserved.

Examination of this notion is presented in Figure 16, in which the percent difference in scattered energy after FVM discretization is plotted versus the number of solid angle sub-angles. The continuous angular variation is discretized into M = 24-288 discrete directions, and each solid angle is subdivided into ($N_{s\phi}$ x $N_{s\theta}$) sub-angles, with $N_{s\phi}$= $N_{s\theta}$, ranging from (2 x 2) to (24 x 24) divisions. Results are presented for the HG phase function with asymmetry factor g = 0.9300.

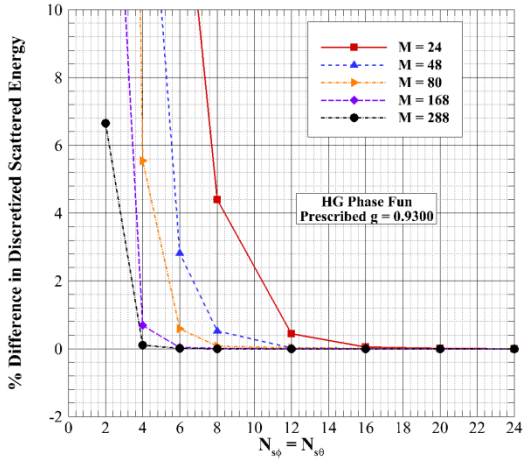

Figure 16: Examination of percent difference in scattered energy conservation versus solid-angle splitting number for HG g = 0.9300 for FVM (reproduced from [77])

For a given discrete direction number, increase in solid-angle splitting resolution reduces the discrepancy in scattered energy conservation. In order to conserve scattered energy accurately within 0.001%, (24 x 24), (20 x 20), (20 x 20), (12 x 12), and (12 x 12) sub-angles are required for M = 24, 48, 80, 168, and 288, respectively. The results in Figure 16 appear to support the theory that solid-angle splitting can accurately conserve scattered energy without requiring additional phase-function treatment. However, care must be taken to ensure that a fine-enough sub-angle density is applied.

The phase-function asymmetry factor conservation of Eq. (11) can be reformulated for the FVM as follows:

$$\frac{1}{4\pi}\sum_{l=1}^{M}\bar{\Phi}^{l'l}\cos\Theta^{l'l}\,\Delta\Omega^{l}=g\,,\qquad l'=1,2,\ldots,M \tag{20}$$

Would the solid-angle splitting technique of Chui et al. [40] accurately conserve phase-function asymmetry factor? Figure 17 illustrates the deviation from asymmetry factor conservation with various FVM discrete directions and angle splitting levels for a prescribed HG g = 0.9300. For lower amounts of sub-angles, significant deviations from asymmetry factor conservation are witnessed for all directional quadratures. However, instead of converging towards 0% as seen in Figure 16, discretized asymmetry factors converge to a value slightly less than the prescribed g = 0.9300. For (24 x 24) splitting, the discretized asymmetry factors for M = 24-288 are g = 0.8855, 0.9024, 0.9113, 0.9198, and 0.9237, respectively, indicating that asymmetry factor is not accurately conserved, and that solid-angle splitting is not sufficient to accurately satisfy Eqs. (19) and (20) concurrently. Thus, additional treatment is required to ensure that angular false scattering errors are mitigated in radiative transfer computation using the FVM.

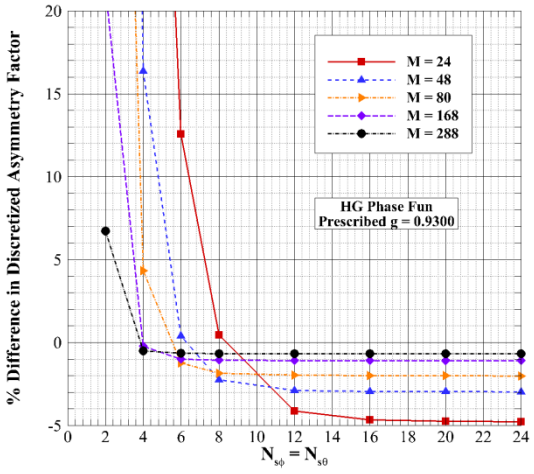

Figure 17: Examination of percent difference in asymmetry factor conservation versus solid-angle splitting number for HG g = 0.9300 for FVM (reproduced from [77])

In order to correct the deviations in asymmetry factor, Hunter and Guo's 2012 normalization can be applied for the FVM, as follows:

$$\tilde{\Phi}^{l'l}=\left(1+A^{l'l}\right)\bar{\Phi}^{l'l} \tag{21}$$

where $\tilde{\Phi}^{l'l}$ satisfies Eqs. (19) and (20), along with directional symmetry. Other than the use of the averaged scattering phase-function, determination of the normalization parameters is identical for the FVM and DOM.

An analysis of the impact of proper phase-function normalization for the FVM is presented in Figure 18, in which the same problem addressed in Figure 5 for the DOM is examined. Heat fluxes at the far wall are generated using the FVM with M = 168 discrete directions both with and without Hunter and Guo's 2012 normalization. (16 x 16) solid angle splitting is implemented for both FVM profiles. As before, benchmark MC predictions are presented, for comparison.

As witnessed for the DOM with scattered energy normalization in Figure 5, FVM profiles are nearly identical for weakly-forward scattering, reinforcing the notion that normalization is ultimately unnecessary at low g. For g = 0.8000, heat flux generated using Hunter and Guo's 2012 normalization results in 0-2% overpredictions of the benchmark MC, while non-normalization leads to 1-3% underpredictions. For this asymmetry factor, both heat flux profiles can be considered as accurate with respect to MC. For g = 0.9300, however, noticeable improvements are witnessed after application of Hunter and Guo's 2012 normalization. Normalization reduces error with respect to MC to less than 2% for all locations except near x^* = 0, where maximum differences are ~5%. Conversely, lack of asymmetry factor leads to 6-12% underpredictions in radiative heat flux, corresponding to a 14.6% scattering effect change from the prescribed g = 0.9300 to the discretized g = 0.9198.

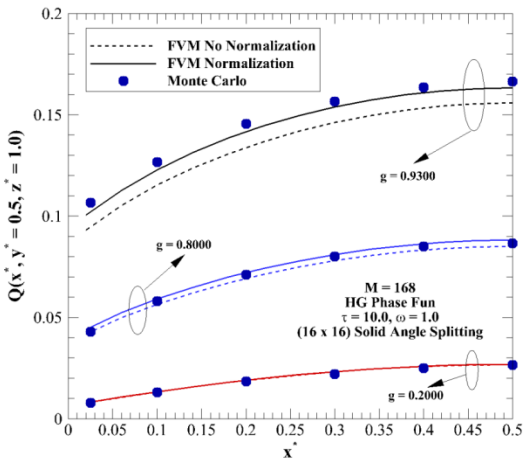

Figure 18: Q(x*, y* = 0.5, z* = 1.0) generated using FVM with and without Hunter and Guo's 2012 normalization with (16 x 16) angle splitting and comparison with MC [62] for HG g = 0.2000, 0.8000, and 0.9300

Figure 19 investigates the impact of angular resolution on FVM heat flux with g = 0.9300. Heat fluxes are again presented both with and without Hunter and Guo's 2012 normalization, using (16 x 16) splitting. The number of discrete directions is varied between M = 24, 48, 80, and 168. When normalization is ignored, angular false scattering is prevalent, with large differences between FVM and MC witnessed (~12% for M = 168). Application of normalization improves conformity greatly for all quadratures (< 4%) except the lowest order, where a difference of 30% is still witnessed near the wall center. The underlying cause of this large discrepancy near the wall stems mainly from ray effect, due to the fact that the angular discretization is too fine. As discrete direction number is increased, ray effect is sufficiently mitigated, and conformity between FVM and MC after application of normalization is excellent.

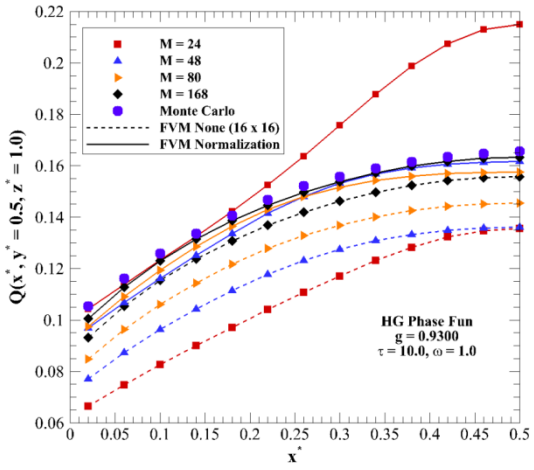

Figure 19: Q(x*, y* = 0.5, z* = 1.0) generated using FVM with and without Hunter and Guo 2012 normalization with (16 x 16) angle splitting and comparison with MC [62] for various discrete direction numbers with HG g = 0.9300

The ability of Hunter and Guo's 2012 normalization to accurately conserve scattered energy and asymmetry factor simultaneously offers the possibility that radiative transfer accuracy can be retained with substantial reduction in solid-angle splitting density. This notion is examined in Figure 20, where the percent difference in FVM heat flux $Q(x^*, y^* = 0.5, z^* = 1.0)$ from the benchmark MC solution is presented for M = 168 and various solid angle splitting densities. FVM profiles generated with no normalization are presented for splitting levels ranging between (6 x 6) and (24 x 24), while FVM profiles generated using Hunter and Guo's 2012 normalization are presented using (2 x 2) and (24 x 24) solid angle splitting.

When normalization is ignored, increasing solid-angle splitting density results in convergence of FVM heat flux profiles, due to more accurate conservation of scattered energy. However, even at (24 x 24) splitting, non-normalized FVM profiles underpredict MC by between 6-12%, corresponding to the discretized g = 0.9198. When normalization is implemented, (24 x 24) splitting results in FVM conforming to MC within 4%. Of greater importance, however, is the fact that the FVM profile generated with minimal (2 x 2) splitting is nearly identical to (24 x 24). This indicates that further solid-angle splitting past (2 x 2) is not required to obtain accurate radiation transfer solutions when normalization is implemented.

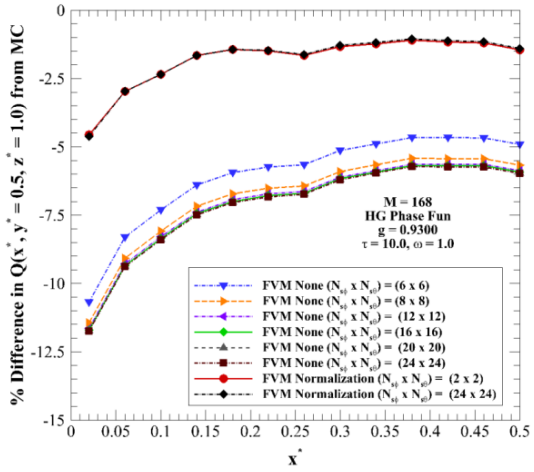

Figure 20: Percentage difference with MC [62] of Q(x*, y* = 0.5, z* = 1.0) generated using FVM with and without Hunter and Guo's 2012 normalization with various solid angle splitting levels with M = 168

The ability to reduce the number of divisions per control-volume solid angle from (24 x 24) to (2 x 2), while maintaining radiative transfer accuracy, is extremely important in terms of computational efficiency. For M = 168, it takes 1935 seconds to perform the solid-angle splitting procedure using $(N_{s\phi}$ x $N_{s\theta})$ = (24 x 24), while it takes less than 1 sec using $(N_{s\phi}$ x $N_{s\theta})$ = (2 x 2) (a reduction of almost 100%). Implementation of Hunter and Guo's 2012 normalization thus has the distinct advantage of being able to produce accurate FVM radiative transfer predictions while maximizing computational efficiency.

As discussed earlier for the DOM, the fact that the number of discrete directions is unlimited in the FVM puts forth the possibility that scattered energy and asymmetry factor can both be conserved simultaneously without normalization, assuming a large enough number of directions is used for analysis. This concept is addressed in Figure 21, which plots FVM heat flux profiles, generated with extremely high discrete direction numbers and no normalization, and compares them with the benchmark MC values. In addition to high-direction FVM profiles, FVM solutions generated using Hunter and Guo's 2012 normalization at lower discrete direction numbers (M = 168 and 288) are plotted. Interestingly, the normalized FVM profiles are more accurate with respect to MC than the three extreme cases, with average percent differences of less than 2%. Using (2 x 2) splitting, these two heat flux profiles can be generated in 497 and 1341 seconds, respectively. Without normalization, generating heat fluxes using M = 624, 1088, and 2024 discrete directions takes 5650, 16520, and 65400 seconds. Thus, while substantial increase in discrete

direction number can effectively minimize angular false scattering, use of Hunter and Guo's 2012 normalization is much more practical.

The results in this section show that phase-function normalization is a practical tool for determining radiative heat transfer in anisotropic media regardless of the numerical method implemented (DOM or FVM), as long as normalization accurately conserves scattered energy and asymmetry factor concurrently after discretization.

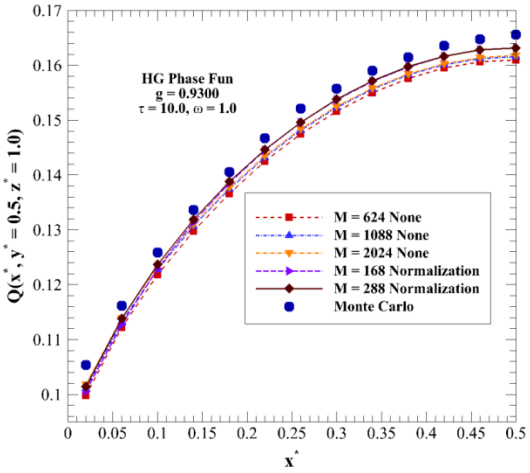

Figure 21: Comparison of Q(x*, y* = 0.5, z* = 1.0) between MC solutions [62] and FVM solutions with and without Hunter and Guo 2012 normalization using extremely high-order quadrature

PHASE-FUNCTION NORMALIZATION FOR BALLISTIC RADIATION

For problems involving ballistic radiation, care must be taken to ensure that the discretized ballistic scattering phase functions satisfy scattered energy conservation, as well as asymmetry factor conservation. Using the FVM as an example, with solid-angle splitting, the ballistic scattered energy and asymmetry factor conservation conditions can be written as follows:

$$\frac{1}{4\pi}\sum_{l=1}^{M}\bar{\Phi}^{l^B l}\Delta\Omega^{l}=1 \tag{22a}$$

$$\frac{1}{4\pi}\sum_{l=1}^{M}\bar{\Phi}^{l^B l}\cos\Theta^{l^B l}\,\Delta\Omega^{l}=g \tag{22b}$$

When the ballistic direction coincides with one of the discrete directions, we can directly use the normalization parameters associated with the ballistic direction from the diffuse radiation normalization. In such cases, the features with diffuse radiation normalization such as occurrence of negative phase function values in the three simpler normalization techniques still hold. It should be noted that the direction of ballistic incidence $\hat{\boldsymbol{s}}^{l^B}$ may not coincide with any of the discrete directions inherent in the FVM quadrature set, and thus these additional constraints on ballistic phase-function are required. Similar conditions for the DOM can be written by replacing the discrete solid angle $\Delta\Omega^{l}$ with the DOM weighting factor w^{l}, and by removing the averaging bar from the ballistic scattering phase function.

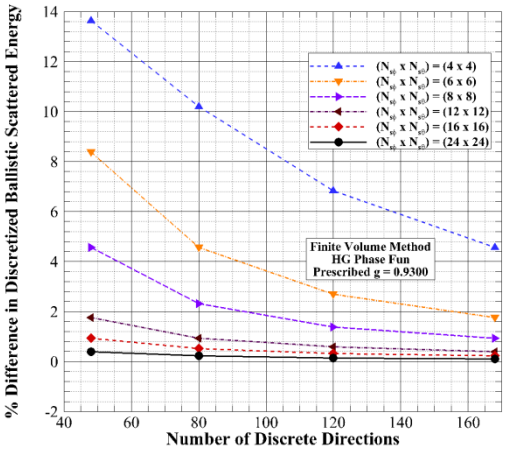

(a)

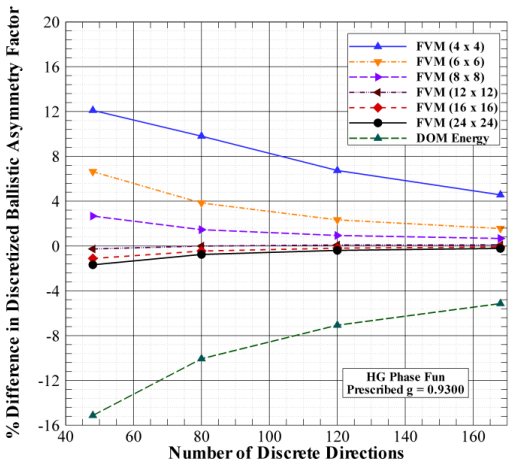

(b)

Figure 22: Percentage difference from a) ballistic scattered energy conservation and b) ballistic asymmetry factor conservation with various discrete directions and splitting levels for HG phase function with g = 0.9300

It is crucial to investigate the impact of solid-angle splitting of the FVM quadrature on the conservation of ballistic scattered energy in the system. Figure 22a displays the deviation of ballistic scattered energy conservation after FVM discretization using M = 48, 80, 120, and 168 discrete directions. As in Figure 16 for diffuse radiation, each solid-angle is split into numerous sub-angles, with splitting level ranging from (4 x 4) to (24 x 24). Ballistic scattered energy values are presented for the ballistic radiation direction with polar angle $\theta = 0°$ (i.e., $\hat{\boldsymbol{s}}^{l^B} = 0\hat{\boldsymbol{\imath}} + 0\hat{\boldsymbol{\jmath}} + 1\hat{\boldsymbol{k}}$) using the HG phase function approximation with g = 0.9300. The exact direction of ballistic incidence will result in slight differences in

ballistic scattered energy deviations [57], and hence, for brevity, values only for the vertical ballistic incident direction are presented.

For a given discrete direction number M, increase in solid-angle splitting density results in convergence of ballistic scattered energy deviations towards zero. For (4 x 4) splitting, ballistic scattered energy deviates greatly from accurate conservation, with differences ranging between 5-13%. In order to obtain accurate conservation within 0.5%, splitting levels of (24 x 24), (24 x 24), (16 x 16), and (12 x 12) are required for M = 48, 80, 120, and 168, respectively. At high resolution of (24 x 24), deviations from energy conservation are less than 0.4% for all quadratures, indicating that use of sufficient solid-angle splitting is able to conserve ballistic scattered energy effectively after FVM directional discretization, similar to the results witnessed for diffuse radiation in Figure 16.

For the same directional quadratures and splitting levels, Figure 22b investigates the conservation of ballistic asymmetry factor after directional discretization for the HG g = 0.9300 phase function. For low solid-angle splitting, deviations in asymmetry factor are noticeable for all quadratures. When (6 x 6) splitting is used, the discretized g for ballistic radiation is altered from g = 0.9300 to 0.9916, 0.9658, 0.9517, and 0.9445 for M = 48, 80, 120, and 168, respectively. As splitting is increased, the discretized ballistic asymmetry factor values start to converge towards the prescribed value, but then overshoot and underpredict. For example, for (24 x 24) splitting, discretized g values of 0.9144, 0.9230, 0.9264, and 0.9280 are witnessed for the four direction numbers. As seen for diffuse radiation, small deviations in asymmetry factor can lead to large errors due to angular false scattering. Thus, for ballistic radiation, additional phase-function treatment is required to ensure the accurate satisfaction of Eqs. (22a) and (22b).

Hunter and Guo's 2012 Normalization for Ballistic Radiation

Phase-function normalization of the ballistic scattering phase function $\Phi^{l^B l}$ is independent of the diffuse scattering phase function normalization presented earlier, except for the case when the direction of ballistic incidence corresponds directly to one of the discrete quadrature directions. In order to ensure conservation of ballistic scattered energy and asymmetry factor, Hunter and Guo's 2012 normalization can be reformulated for ballistic radiation as follows:

$$\widetilde{\Phi}^{l^B l} = (1 + A^{l^B l})\overline{\Phi}^{l^B l} \tag{23a}$$

$$\frac{1}{4\pi}\sum_{l=1}^{M} \widetilde{\Phi}^{l^B l}\Delta\Omega^l = 1 \tag{23b}$$

$$\frac{1}{4\pi}\sum_{l=1}^{M} \widetilde{\Phi}^{l^B l}\cos\left(\Theta^{l^B l}\right)\Delta\Omega^l = g \tag{23c}$$

where the ballistic normalization vector $A^{l^B l}$ are generally independent of the normalization matrix $A^{l' l}$ in Eq. (16). The minimum norm solution of the above system of equations will generate the normalization parameters $A^{l^B l}$ that will accurately conserve ballistic scattered energy and asymmetry factor.

While Figures 22a-b provide the mathematical reasoning behind applying ballistic phase-function normalization to ensure conservation of ballistic scattered energy and asymmetry factor, an analysis of radiative transfer is required to further show the necessity of such a treatment to avoid angular false scattering errors. The test problems for the forthcoming analyses involve ultrafast radiation transfer in the cubic enclosure described earlier. For all simulations, time is non-dimensionalized as $t^* = ct/L$. For all analyses, the medium is taken to be cold, and the wall boundary conditions and optical properties of the medium vary depending on the analysis. For ultrafast simulation, it is critical that the non-dimensional time step is small enough to ensure that the traveling distance of light between successive time steps is less than the size of a single control-volume. Using a (27 x 27 x 27) spatial grid, the temporal time step for all analyses is taken as Δt^* = 0.03.

It is crucial to mention that the forthcoming analyses are being performed solely to investigate the impact of ballistic phase function normalization for ultrafast radiative transfer. Regarding the treatment of $\Phi^{l' l}$, Hunter and Guo's 2012 normalization is applied in all simulations to minimize angular false scattering errors and place the focus of this section solely on ballistic normalization.

The first test problem involves a purely scattering (ω = 1.0), anisotropically scattering (HG g = 0.9300) medium, with optical thickness τ = 1.0. All enclosure walls taken as cold and black, while the wall at z^* = 0 is irradiated by a normal, collimated incidence of unity intensity. The energy propagation through the medium is visualized by investigating heat flux at the centerline of the opposing wall, or $Q(x^*, y^* = 0.5, z^* = 1.0)$. For this benchmark problem, reference steady-state MC solutions are available in Collin et al. [63]. Comparison of FVM and DOM predictions with and without ballistic phase-function normalization with reference MC solutions will help illustrate the necessity for accurate conservation of Eq. (22a) and (22b).

Figure 23 investigates the impact of ballistic phase function normalization on ultrafast heat flux at different non-dimensional times for both the DOM and FVM using M = 80 discrete directions. Heat fluxes are generated using the DOM with two ballistic normalization approaches: 1) using scattered energy normalization, similar to Eq. (10), to conserve ballistic scattered energy only, and 2) using Hunter and Guo's 2012 normalization. FVM profiles are presented with and without Hunter and Guo's 2012 normalization. When normalization is ignored, FVM profiles are presented for both (6 x 6) and (24 x 24) solid-angle splitting.

DOM heat flux generated using scattered energy normalization to conserve ballistic scattered energy deviates greatly from all other profiles, including the reference MC solution at large t^*, due to the fact that ballistic asymmetry factor is altered from g = 0.9300 to 0.8364. The artificial

reduction of asymmetry factor results in lower heat fluxes at the opposite wall, due to the fact that energy does not scatter as strongly in the forward direction. For the DOM, application of Hunter and Guo's 2012 normalization for ballistic radiation is able to conserve ballistic asymmetry factor, which markedly improves heat fluxes as compared with FVM and MC. Implementation of Hunter and Guo's 2012 normalization reduces differences at the wall center (x^*= 0.5) with respect to MC at large t^* from 7.5% when ballistic scattered normalization is applied to 0.5%. Near the wall, large differences between DOM and MC are witnessed, which can be attributed to both spatial and angular discretization. However, accurate conformity far from the wall indicates accuracy improvement due to ballistic asymmetry factor conservation.

.

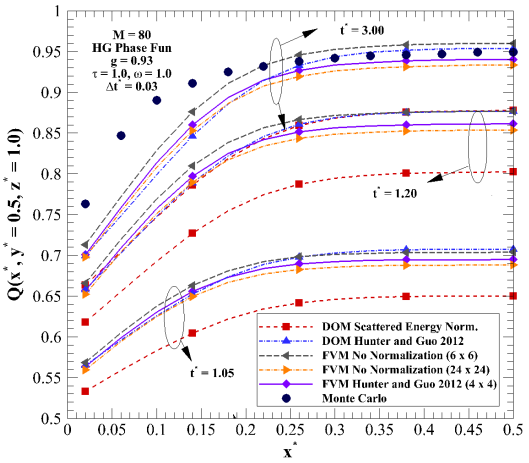

Figure 23: Impact of ballistic normalization on Q(x*, y* = 0.5, z* = 1) at various time instants for normal ballistic incidence at z* = 0 wall at various times using DOM and FVM with M = 80 and comparison with MC [63])

For all non-dimensional times, DOM profiles generated with Hunter and Guo's 2012 normalization for ballistic radiation conform accurately to FVM profiles using the same normalization approach. Differences near the wall center are less than 1.9% at all non-dimensional times. The conformity of the two different numerical methods to one another, as well as steady-state accuracy when compared to MC, reinforces the premise that conservation of ballistic scattered energy and asymmetry factor simultaneously will result in improved accuracy of ultrafast radiation transfer in anisotropically scattering media, due to reduction of angular false scattering.

Additionally, heat flux profiles are presented for the FVM without normalization using (6 x 6) and (24 x 24) solid-angle splitting. The percent difference between the (6 x 6) FVM and FVM with Hunter and Guo's 2012 normalization at x^* = 0.5 range between 1.3-2.1%, depending on non-dimensional times. By contrast, when (24 x 24) splitting is used, these differences drop to between 0.7-0.95%. The reduction in discrepancy conforms to the data shown in Figures 22a and 22b, as refinement of splitting number reduces discrepancies in ballistic scattered energy and asymmetry factor conservation. A caution: at t^* = 3.0, heat flux generated using FVM with (6 x 6) splitting appears to conform more accurately to MC than (24 x 24). However, at this splitting level, ballistic scattered energy is not accurately conserved, as seen in Figure 22a, and thus this result holds no meaning.

Figure 24 illustrates the impact of varying solid-angle splitting levels on the percent difference between FVM heat flux and MC at large t^* for the problem illustrated in Figure 23, with M = 168. When normalization is ignored, a general converging trend in the FVM to MC percent differences is witnessed with increase in solid-angle splitting. For (24 x 24) splitting, ballistic scattered energy is accurately conserved, and a 1.2% underprediction at x^*= 0.5 is witnessed with respect to FVM. When Hunter and Guo's 2012 normalization is implemented with (24 x 24) splitting, the difference at the center reduces to 1.0%, indicating minimal improvement. Of more importance, however, is the fact that normalized FVM heat flux with (4 x 4) splitting is nearly identical to that generated with (24 x 24) splitting, with a maximum difference of only 0.05%. This indicates that use of Hunter and Guo's 2012 normalization for ballistic radiation produces similar FVM heat fluxes regardless of splitting level, allowing for a major reduction in computational time. For M = 168, it takes 1935 seconds to perform (24 x 24) splitting, while for (4 x 4) splitting, only 1.4 seconds are required. Implementation of Hunter and Guo's 2012 normalization for ballistic radiation thus has the distinct advantage of being able to produce accurate radiation transfer solutions while maximizing computational efficiency. Additionally, DOM heat fluxes determined using Hunter and Guo's 2012 normalization conform accurately to FVM within a few percent, indicating that normalization produces similar heat flux profiles regardless of numerical technique.

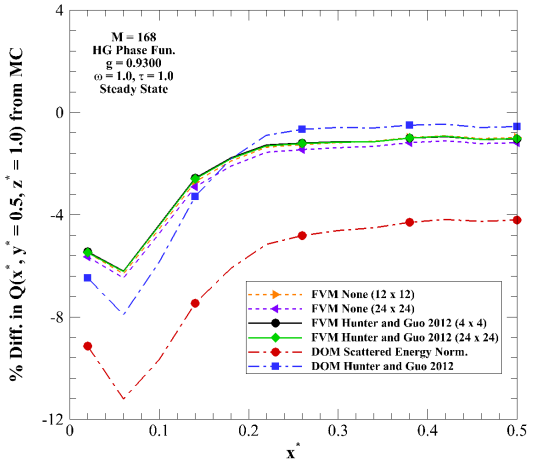

Figure 24: Percent difference in Q(x*, y* = 0.5, z* = 1) between MC FVM solutions both with and without Hunter and Guo's 2012 normalization using various solid angle splitting densities for M = 168 directions

The previous benchmark analysis gives an indication of the importance of conserving both ballistic scattered energy and asymmetry factor. To further support the necessity of such treatment, analysis of ultrafast radiative transfer in a tissue-like

medium is presented in Figures 25-28. For ultrafast radiation applications involving biological tissue, such as laser hyperthermia for cancer irradiation, accurate prediction of the amount of radiant energy absorbed by both cancerous and healthy tissues is paramount, as incorrect analysis of energy deposition could lead to either thermal damage and/or necrosis of healthy biological tissue during irradiation, or improper eradication of cancerous tissue. Thus, it is of great importance to gauge the impact of ballistic normalization on the divergence of heat flux (or energy deposition) in a biological tissue medium, so that numerical simulations will be accurate. The divergence of heat flux can be calculated using the following formula:

$$\nabla \cdot q_r = \tau(1-\omega)(4\pi I_b - G) \tag{24}$$

where G is the incident radiation.

For Figures 25-28, the benchmark problem involves a cubic enclosure with optical properties similar to human dermis [78]: τ = 18.97, ω = 0.9858. The asymmetry factor is taken as g = 0.9300. As in the previous test problem, the wall at z^* = 0 is irradiated by a normal, collimated incidence of unity intensity. The remaining walls, and medium as well, are taken as cold. At z^* = 0, a Fresnel reflection boundary condition is imposed [36], in order to account for the mismatch of refractive index between tissue and air. All other enclosure walls are taken as diffuse reflectors, with diffuse reflectivity of 0.5, due to the highly scattering optical thickness of turbid tissue and the theory of random walk [49].

Figure 25 illustrates the impact of ballistic normalization on the ultrafast divergence of heat flux in the tissue medium at various non-dimensional times using both DOM and FVM with and without Hunter and Guo's 2012 normalization. Energy deposition profiles are taken along a line perpendicular to the incident surface and passing through the cube center, i.e. $\nabla \cdot q_r(x^* = 0.5, y^* = 0.5, z^*)$. Divergence profiles are generated using M = 80 discrete directions.

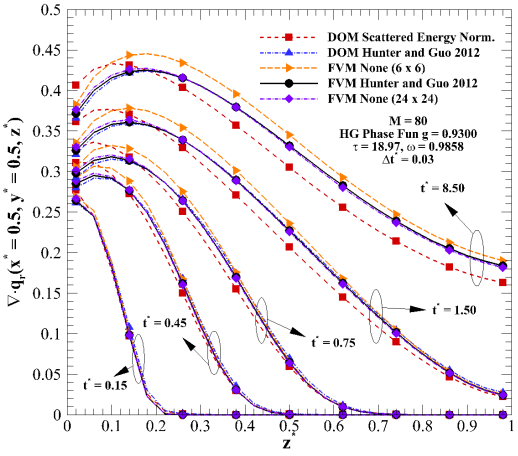

Figure 25: Impact of ballistic normalization on $\nabla \cdot q_r$ (x*=0.5,y*=0.5,z*) at different non-dimensional times using DOM and FVM with M = 80 directions in a medium with tissue-mimicking properties

Energy absorption increases at all medium locations with increase in non-dimensional time. For early times, energy absorbed deep in the medium is negligible, due to the high optical thickness of tissue preventing easy passage of radiant energy through the medium. Large discrepancies are witnessed between energy deposition calculated using the DOM with scattered energy normalization for ballistic radiation and the DOM with Hunter and Guo's 2012 normalization for ballistic radiation. Near the incident wall (x^* = 0.02), DOM with scattered energy normalization overpredicts Hunter and Guo's 2012 normalization by ~11% at all non-dimensional times. Further into the medium, underpredictions of between 11-23% exist. These results conform to the alteration of discretized ballistic asymmetry factor from g = 0.9300 to 0.8364 when scattered energy normalization is applied to the ballistic phase function. A reduction in g results in radiant energy being scattered in a less strong-forward fashion, leading to higher energy deposition near the source and lower deposition far from the source.

The impact of solid-angle splitting for the FVM without ballistic normalization can be clearly witnessed in Figure 25. When minimal solid-angle splitting of (6 x 6) is implemented, the discretized g is altered to 0.9658, leading to larger energy depositions at all t^* as compared to the FVM with Hunter and Guo's 2012 normalization for ballistic radiation. Overpredictions of maximums of 11.5%, 4.8%, and 4.7% are witnessed for t^* = 0.45, 1.50, and 8.50, respectively, indicating that increase in time reduces discrepancies caused by angular false scattering. When splitting is increased to (24 x 24), maximum differences between normalized and non-normalized FVM reduce to 7.4%, 2.1%, and 1.1% at the three non-dimensional times, respectively. The discretized g = 0.9280 for this splitting, indicating that the minimal deviation in g has a large impact at lower times, but minimal impact as steady-state approaches. Accurate conformity between the DOM and FVM is witnessed when Hunter and Guo's 2012 normalization is applied to both approximate methods, with a maximum difference of only 1.5% occurring at t^* = 8.50.

Expanding on the results in Figure 25, Figure 26 explores contours of percent difference in divergence of radiative heat flux $\nabla \cdot q_r(x^*, y^* = 0.5, z^*)$ along a plane cutting through the center of the cubic enclosure calculated using the DOM with M = 80 both with scattered energy normalization and Hunter and Guo's 2012 normalization for ballistic radiation. Near the source at z^* = 0.02, the DOM with scattered energy normalization overpredicts Hunter and Guo's 2012 normalization by between 9-12%, depending on x^*. Conversely, as the distance from the source wall increases, DOM with scattered energy normalization begins to underpredict with respect to Hunter and Guo's 2012 normalization, due to lack of energy propagation stemming from a reduction in g. Near the wall opposite from the source (z^* = 0.98), the percent differences range between -10 and -12.

Figure 27 plots similar contours between the FVM with no normalization and (6 x 6) solid-angle splitting and the FVM with Hunter and Guo's 2012 normalization. At all locations, divergence of heat flux generated using FVM with no

normalization overpredicts the normalized results. Differences range between 0-5%, depending on location in the medium. The overpredictions in divergence of heat flux stem from an alteration in g to 0.9658 when (6 x 6) splitting is applied, indicating that ballistic radiation scatters more strongly through the medium in the forward direction.

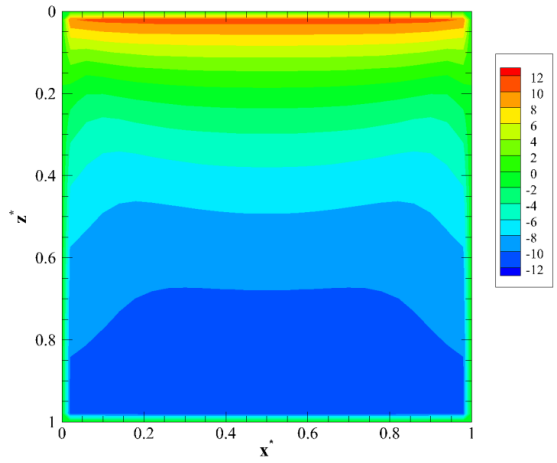

Figure 26: Contours of percentage difference in $\nabla \cdot q_r(x^*, y^* = 0.5, z^*)$ between DOM with ballistic scattered energy normalization and Hunter and Guo's 2012 ballistic normalization for M = 80 in a tissue-mimicking medium

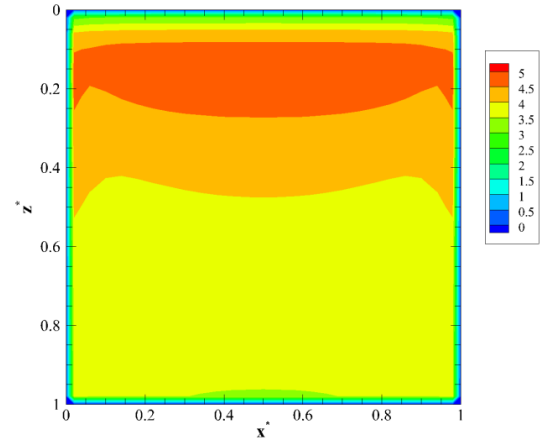

Figure 27: Contours of percentage difference in $\nabla \cdot q_r(x^*, y^* = 0.5, z^*)$ between FVM with no normalization and FVM with Hunter and Guo's 2012 ballistic normalization for M = 80 in a tissue-mimicking medium

The differences in energy deposition witnessed in Figures 26 and 27 due to lack of ballistic asymmetry factor can be crucial for ultrafast biomedical applications. Consider the thermal destruction of cancerous tissue using laser hyperthermia. During this process, it is critical that cancerous tissue is heated to a point where those cells cannot survive, while the surrounding healthy tissue must be protected from excessive thermal damage. An overprediction in divergence of radiative heat flux in the medium could result in cancerous tissue not being totally destroyed in actual experimentation. Conversely, numerical underpredictions due to lack of asymmetry factor conservation could lead to excessive thermal damage and necrosis of healthy tissue.

As an additional means of justifying the use of Hunter and Guo's 2012 normalization for ballistic radiation, Figure 28 presents contours of percentage difference in divergence of heat flux between the DOM and FVM. In both cases, Hunter and Guo's 2012 normalization for ballistic radiation is implemented. Throughout the entire selected slice of tissue, excellent agreement between the DOM and FVM is witnessed, with conformity of less than 1.5% occurring for all locations. The accurate conformity of two different approximate methods after application of Hunter and Guo's 2012 normalization for ballistic radiation gives confidence that both ballistic scattered energy and asymmetry factor are accurately conserved after discretization, leading to improvement in numerically predicted radiative transfer results.

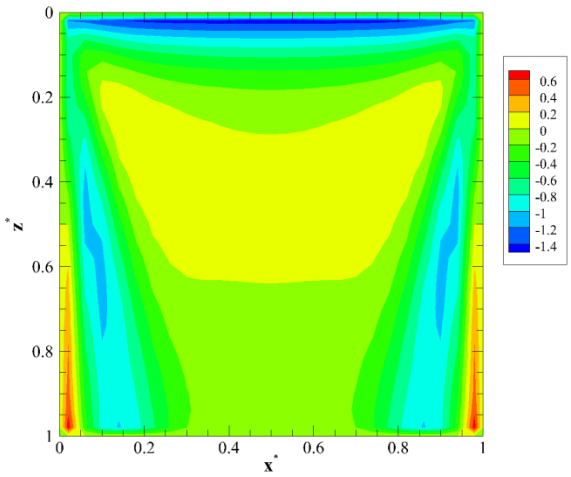

Figure 28: Contours of percentage difference in $\nabla \cdot q_r(x^*, y^* = 0.5, z^*)$ between FVM and DOM with Hunter and Guo's 2012 ballistic normalization applied for M = 80 in a tissue-mimicking medium

Hunter and Guo's 2014 Normalization for Ballistic Radiation

Previously, it was shown that Hunter and Guo's 2014 normalization for diffuse radiation was a simpler alternative to Hunter and Guo's 2012 normalization for HG phase functions (not for Legendre phase functions because it generates negative phase function values). Thus, it is needed to examine this technique in ballistic radiation for HG phase functions only. Formulation of Hunter and Guo's 2014 normalization for ballistic radiation, however, becomes more complicated. Due to the non-flexibility of DOM quadrature, if the ballistic radiation does not correspond directly to one of the DOM directions, no forward- or backward-scattering ballistic phase function term will exist, as directions with $\cos\Theta^{l^{B_l}} = \pm 1$ will not exist. In order to apply Hunter and Guo's 2014 normalization for ballistic radiation, the phase function for the

directions where $\cos\Theta^{l^B l}$ reaches its minimum and maximum can be normalized. Applying this idea, the "forward"- and "backward"-scattering ballistic normalization parameters for Hunter and Guo's 2014 normalization can be written as follows:

$$A^{l^{B+}} = \frac{\left[4\pi\left(\cos\Theta^{l^B l^{B-}} - g\right) + \sum_{l=1}^{M} \Phi^{l^B l} w^l \left(\cos\Theta^{l^B l} - \cos\Theta^{l^B l^{B-}}\right)\right]}{\left[N^{B+}\Phi^{l^B l^{B+}} w^{l^{B+}}\left(\cos\Theta^{l^B l^{B-}} - \cos\Theta^{l^B l^{B+}}\right)\right]} \quad (25a)$$

$$B^{l^{B-}} = \frac{\left[4\pi\left(\cos\Theta^{l^B l^{B+}} - g\right) + \sum_{l=1}^{M} \Phi^{l^B l} w^l \left(\cos\Theta^{l^B l} - \cos\Theta^{l^B l^{B+}}\right)\right]}{\left[N^{B-}\Phi^{l^B l^{B-}} w^{l^{B-}}\left(\cos\Theta^{l^B l^{B+}} - \cos\Theta^{l^B l^{B-}}\right)\right]} \quad (25b)$$

In the preceding, the directional superscripts l^{B+} and l^{B-} represent the discrete directions that have the maximum and minimum scattering cosine as compared to the direction of ballistic incidence, and the factors N^{B+} and N^{B-} represent the number of discrete directions that attain such a maximum and minimum, respectively. Due to DOM directional symmetry, multiple directions may share the same overall ballistic scattering cosine, and thus addition of these factors is necessary. Using Hunter and Guo's 2014 normalization, care must be taken to normalize every direction that attains the maximum or minimum direction cosine using Eqs. (25a) and (25b).

A similar redefinition must be addressed for Mishchenko's E and Kamdem Tagne's g normalizations for ballistic radiation, in the absence of a true forward-scattering term. Using the ideology explained above, the "forward"-scattering parameters $A^{l^{B+}}$ for ballistic radiation for these two normalization approaches become:

$$A^{l^{B+}} = \frac{\left[4\pi - \sum_{l=1}^{M} \Phi^{l^B l} w^l\right]}{N^{B+}\Phi^{l^B l^{B+}} w^{l^{B+}}} \quad (26a)$$

$$A^{l^{B+}} = \frac{\left[4\pi g - \sum_{l=1}^{M} \Phi^{l^B l} w^l \cos\Theta^{l^B l}\right]}{N^{B+}\Phi^{l^B l^{B+}} w^{l^{B+}} \cos\Theta^{l^B l^{B+}}} \quad (26b)$$

where Eq. (26a) are the parameters for Mishchenko's E normalization, and Eq. (26b) are the parameters for Kamdem Tagne's g normalization.

In Figure 29a, the forward- and backward- scattering normalization parameters for ballistic radiation, generated using Hunter and Guo's 2014 normalization, are presented for varying DOM discrete direction number and quadrature scheme. Parameters are presented for a prescribed HG g = 0.9300. As the HG phase function depends solely on asymmetry factor, and both Hunter and Guo's 2012 and 2014 normalizations are suitable for HG phase-functions of diffuse radiation, the HG phase function is chosen to simplify this analysis. For all directional orders, the forward-scattering normalization parameters attain positive values. Ballistic radiation normalization using the other three normalization approaches result in similar forward-scattering normalization parameters. Examination of the backward-scattering normalization parameters in Figure 29a, however, reveal a crucial issue: parameters are < -1 for nearly all tested quadrature schemes and discrete directions numbers. This means that negative values of $\Phi^{l^B l}$ will exist, and additional treatment will be necessary to avoid negative intensities.

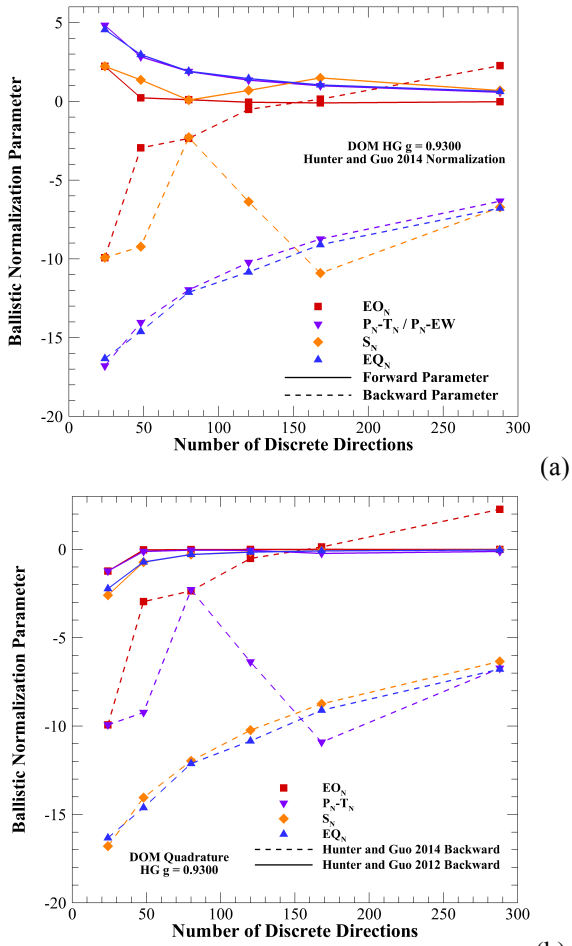

Figure 29: a) The forward and backward normalization parameters for ballistic radiation using Hunter and Guo's 2014 technique and b) comparison of backward-scattering normalization parameters between Hunter and Guo's 2012 and 2014 techniques for ballistic radiation for HG phase-function with g = 0.9300

In Figure 29b, the backward-scattering normalization parameters for ballistic radiation generated using Hunter and Guo's 2014 normalization are compared to those generated using Hunter and Guo's 2012 normalization for the same discrete directions. For Hunter and Guo's 2012 normalization, parameters of < -1 occur only for the lowest order quadrature (N = 4), in stark contrast to Hunter and Guo's 2014 normalization, where parameters < -1 are common, even for N = 16 for the S_N, EQ_N, and P_N-T_N quadratures. It appears that

alteration of every value of $\Phi^{l^B l}$ in Hunter and Guo's 2012 normalization allows for a less substantial alteration of the backward-scattering terms, indicating that it is a more suitable option for normalization of the ballistic radiation scattering phase function.

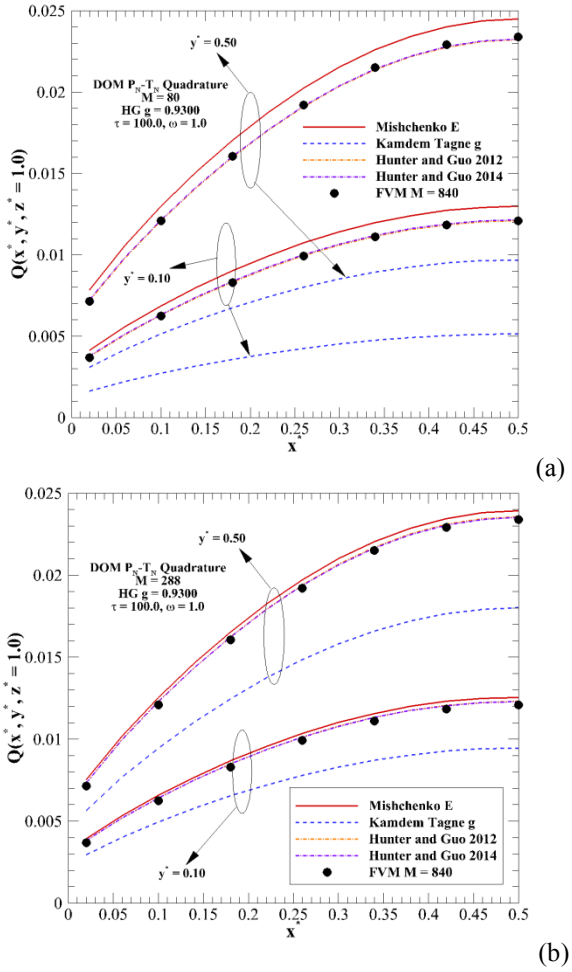

Figure 30: Comparison of heat flux Q(x^*, y^*, z^* = 1.0) profiles generated with FVM and various DOM ballistic radiation normalization techniques in an optically thick medium with a) M = 80 and b) M = 288

The highly negative backward-scattering parameters in Hunter and Guo's 2014 normalization result in negative intensities in the iterative solution of the TERT, which require negative intensity correction. Unlike the diffuse case, in which negative intensities disappeared as radiation penetration increased into the cold medium, negative intensities for ballistic radiation reappear at every iteration step. This is due, in part, to the treatment of ballistic radiation intensity using the Beer-Lambert Law in the solution of the ERT, as the ballistic radiative intensities are given a set value depending on optical depth. Analysis of the impact of these highly-negative normalization parameters is presented in Figures 30(a-b), in which non-dimensional heat fluxes $Q(x^*, y^*, z^* = 1.0)$ in the first benchmark problem are examined for an optically thick (τ = 100), purely scattering (ω = 1.0) medium, with HG g = 0.9300. Results are presented for M = 80 in Figure 30a, and for M = 288 in Figure 30b. DOM heat flux profiles generated using the four ballistic normalization approaches are compared to high-direction FVM to gauge their accuracy.

Hunter and Guo's 2012 and 2014 normalizations result in nearly identical DOM heat flux profiles for both direction numbers. Additionally, these heat fluxes conform accurately within 2% to high-order FVM, indicating their accuracy. Results generated using Mishchenko's E and Kamdem Tagne's g exhibit stronger discrepancies. Lack of asymmetry factor conservation in Mishchenko's E leads to overpredictions of up to 12% and 8% as compared to FVM for M = 80 and 288, respectively. More drastically, lack of energy conservation in Kamdem Tagne's g normalization results in extreme underpredictions of > 55% and > 20% as compared with FVM for M = 80 and 288. This illustrates the crucial importance of ballistic energy conservation for applications involving optically thick media. Although negative intensities are encountered, requiring negative intensity correction, radiative transfer predictions do not seem to be greatly impacted. This is due to the fact that negative intensities only occur in one or a few discrete directions, meaning that the overall effect is minimal.

Finally it should be mentioned that, for normal, ballistic incidence, ballistic forward normalization parameters of < -1 do not appear for Mishchenko's E, Kamdem Tagne's g, and Hunter and Guo's 2014 ballistic normalizations with HG phase functions. For the cases where the direction of ballistic incidence matches one of the predetermined quadrature directions, however, the ballistic normalization parameters will be identical to the diffuse normalization parameters for that quadrature direction. In such cases, diffuse forward parameters of <-1 occur for these three simpler diffuse normalization approaches for certain directions; and thus, the ballistic forward parameters will also be <-1, resulting in negative phase-function values and mandating the necessity of negative intensity correction. Additionally, for ballistic incident directions that are both non-normal and non-aligned with a predetermined quadrature direction, negative forward parameters are encountered for certain Legendre phase-functions. For example, for the EO8 quadrature with the g = 0.8189 Legendre phase-function, a forward ballistic normalization parameter of -1.02 occurs for ballistic incidence at polar angle 43° and azimuthal angle 5° after application of Hunter and Guo's 2014 ballistic normalization. Thus, for general Legendre phase-functions, the existence of negative phase-function values and the necessity of negative intensity correction associated with the simpler normalization techniques is always a concern.

EFFICIENCY COMPARISON OF DOM AND FVM

The results previously described for both the DOM and FVM show that, with proper normalization to conserve scattered energy and asymmetry factor, both numerical methods are able to accurately predict radiative transfer in

anisotropically scattering medium. Results generated for both diffuse radiation and ballistic radiation with both methods conform accurately to Monte Carlo results, as well as to each other.

Recently, some people took for granted preference of the FVM over the DOM simply due to the flexibility of the directional quadrature with FVM. One commonly mentioned disadvantage of the DOM is that the directional quadrature is limited in discrete direction number. With the advent of non-limited quadratures (such as the P_N-T_N) [69], however, this is no longer a concern at all. Certainly, the directions for the DOM do have to satisfy certain moment conditions, making the quadrature choice less flexible than the FVM. On the other side, the satisfaction of the moment conditions makes the distribution of DOM directions more reasonable, particularly under relative lower orders of discrete directions. Therefore, there is no obvious overall advantage of FVM over DOM in terms of directional choice. As for spatial discretization, both methods are based on the finite volume approach and there is no difference between both.

Due to the fact that these two methods are both able to produce accurate radiative transfer results, as shown in this study, it is of interest to examine the computational efficiency of each method. This can be done by analyzing two parameters: 1) computational memory requirement, and 2) computational convergence CPU time. By comparing both computational elements, a better idea on the effectiveness of each method can be garnered.

In Table 2, a comparison of computational time between FVM and DOM is presented for radiative transfer in a 3-D cubic enclosure housing an isotropic, purely scattering, medium with optical thickness τ = 10.0 irradiated by one hot wall at z^* = 0. Computational times (in seconds), as well as the ratio between FVM and DOM times, are presented for varying discrete direction number and spatial grid size. All DOM times are generated using the P_N-T_N quadrature, while FVM times are generated for the FT_N-FVM quadrature.

For a given discrete direction number, an increase in spatial grid density lowers the FVM/DOM time ratio. Additionally, for a given spatial grid, increase in discrete direction number also decreases the FVM/DOM time ratio. At low discrete direction number, the DOM converges significantly faster than the FVM. Even at the highest discrete direction number examined (M = 288), the DOM converges ~5% faster than the FVM for all spatial grid numbers, indicating that the DOM is more computationally efficient in terms of CPU time for this benchmark problem.

In Table 3, computational times are presented for radiative transfer in the same cubic enclosure described in Table 2, except with anisotropic scattering (HG g = 0.9300). The spatial grid is kept constant at (17 x 17 x 17), and the optical thickness is taken to be either τ = 10.0, 50.0, or 100.0. The pattern in FVM/DOM time ratios versus discrete direction number is fairly similar for all three optical thicknesses. For low direction number (M = 24), the DOM is over twice as fast as the FVM. Use of M = 168 and 288 results in the DOM converging ~15% and ~5% faster, respectively, than the FVM, similar to the trend witnessed for isotropic scattering. The conformity of FVM/DOM time ratios between isotropic scattering and anisotropic scattering in Tables 2 and 3, respectively, indicates that the ratios do not vary strongly with optical properties. Instead, they depend mainly on both the angular and spatial grid densities.

The second method of analyzing the computational efficiency of the FVM and DOM is to perform a computational memory comparison. In Table 4, required computation memory (in MB) for both the FVM and DOM are tabulated for various discrete direction numbers and spatial grids in a 3-D cubic medium. Computational memory depends solely on the computational image size (i.e., size of variables and arrays being stored using RAM), and is independent of optical properties and initial/boundary conditions. For all grids and discrete direction numbers in Table 4, the FVM and DOM use nearly identical memory. The ratios for all cases are between 1.00 and 1.01, indicating that either method is efficient in terms of memory. However, combining the results in Table 4 with those in Tables 2 and 3, the DOM is superior in overall efficiency, as it is able to significantly reduce computational time over the FVM for the same problem without reducing accuracy.

An interesting comparison of computational memory is shown in Table 5, in which committed memory (in MB) are presented for radiative transfer in a 2-D, axisymmetric cylindrical enclosure using various discrete direction numbers and spatial grids of (150 x 150), (200 x 200), and (400 x 400). For all three spatial grid numbers, FVM/DOM memory ratios are similar for a given discrete direction number. However, the DOM uses significantly less memory than the FVM for the 2-D axisymmetric case, with FVM/DOM memory ratios ranging between 1.37-1.90 for M = 24-288. The underlying cause of this logarithmic increase in memory ratio with increasing M stems from the treatment of the angular derivative [45]. Classically, the DOM treats the angular derivative using angular differencing coefficients, and thus intensities only need to be saved in two variables: r and z. In the FVM, however, the angular derivative is commonly calculated using neighboring control volumes in the azimuthal direction. Because of this, intensities need to be stored for r, z, and ϕ. The increased dimensionality from 2 in the DOM to 3 in the FVM leads to dramatic increases in array sizes, and therefore, increases in committed memory.

The results from Tables 2-5 indicate that the DOM is a more efficient method, in terms of computational time and memory requirements, than the FVM, especially for situations that can be approximated as axisymmetric, such as laser irradiation of biological tissue and laser material processing. Additionally, the DOM is able to accurately predict radiative transfer in the benchmark problems previously discussed, after application of proper phase-function normalization. The DOM, therefore, should not be dismissed as inferior to the FVM; rather it should be embraced as an accurate, efficient ERT solution methodology.

Table 2: Comparison of computational time (in sec) between FVM and DOM for a 3-D cubic enclosure with one hot wall at $z^* = 0$ housing an isotropic, purely scattering medium with $\tau = 10.0$

	Computational Time (sec)								
	(17 x 17 x 17)			(22 x 22 x 22)			(27 x 27 x 27)		
M	DOM	FVM	Ratio	DOM	FVM	Ratio	DOM	FVM	Ratio
24	1.60	3.43	2.14	6.58	10.2	1.56	16.4	25.3	1.54
48	4.46	8.20	1.84	22.7	31.5	1.39	54.1	73.5	1.36
80	14.5	20.4	1.40	57.2	74.7	1.31	136	170	1.25
168	86.1	104	1.21	285	320	1.12	707	759	1.07
288	345	363	1.05	1001	1055	1.05	2222	2337	1.05

Table 3: Comparison of computational time (in sec) between FVM and DOM for a 3-D cubic enclosure with one hot wall at $z^* = 0$ housing an anisotropic ($g = 0.9300$), purely scattering medium with varying optical thickness

	Computational Time (sec)								
	τ = 10.0			τ = 50.0			τ = 100.0		
M	DOM	FVM	Ratio	DOM	FVM	Ratio	DOM	FVM	Ratio
24	0.89	1.79	2.01	3.96	8.89	2.24	8.62	20.3	2.36
48	2.37	4.12	1.74	11.5	21.4	1.87	26.6	49.0	1.85
80	7.49	10.5	1.40	37.6	53.1	1.41	86.7	124	1.43
168	42.9	49.6	1.16	221	259	1.17	518	602	1.16
288	184	189	1.03	885	924	1.04	2075	2182	1.05

Table 4: Comparison of CPU committed memory (in MB) between FVM and DOM in a 3-D cubic enclosure for various discrete direction numbers and spatial grids

	Computational Memory (MB)								
	(17 x 17 x 17)			(22 x 22 x 22)			(27 x 27 x 27)		
M	DOM	FVM	Ratio	DOM	FVM	Ratio	DOM	FVM	Ratio
24	3.42	3.41	1.00	6.05	6.05	1.00	10.2	10.2	1.00
48	5.25	5.25	1.00	10.0	10.0	1.00	17.4	17.4	1.00
80	7.70	7.75	1.01	15.2	15.3	1.00	27.1	27.2	1.00
168	14.7	14.9	1.01	29.9	30.0	1.00	54.0	54.2	1.00
288	24.6	25.1	1.02	50.3	50.9	1.01	90.8	91.5	1.01

Table 5: Comparison of CPU committed memory (in MB) between FVM and DOM in 2-D, axisymmetric cylindrical enclosure for various discrete direction numbers and spatial grids

	Computational Memory (MB)								
	(150 x 150)			(200 x 200)			(400 x 400)		
M	DOM	FVM	Ratio	DOM	FVM	Ratio	DOM	FVM	Ratio
24	8.91	12.2	1.37	15.6	21.5	1.38	61.5	84.8	1.38
48	13.0	20.5	1.58	22.9	36.1	1.58	90.9	144	1.58
80	25.5	45.3	1.78	45.0	80.2	1.78	179	320	1.79
168	33.7	61.9	1.84	59.7	110	1.84	238	437	1.84
288	56.6	108	1.90	100	191	1.90	399	760	1.90

CONCLUSION

In this study, the necessity of proper phase-function normalization to conserve scattered energy and asymmetry factor in anisotropic scattering media is established, for both the DOM and FVM under both diffuse and ballistic radiation situations. Five normalization approaches are compared, and the following conclusions are made:

1) The commonly directional averaging scattered energy normalization of Eq. (10) for conserving scattered energy does not conserve the phase-function asymmetry factor g generated due to directional discretization. The non-conservation in g result in a third type of numerical error called "angular false scattering" in addition to the well-known ray effect and numerical smearing errors. This new type error is the true "false scattering" because it is the alteration of the medium scattering property. The so-called "false scattering" error in the literature should be appropriately called as "numerical smearing", as it has nothing to do with actual scattering in the medium, but an error of artificial diffusion due to spatial discretization.

2) Two simple normalization approaches of Mishchenko E and Kamdem Tagne g are able to conserve either scattered energy or asymmetry factor via normalization of only the forward-scattering term, but are not able to conserve both. In optically thick media, small deviations in scattered energy conservation in Kamdem Tagne's normalization result in extremely large errors. Additionally, these two approaches suffer from the possibility of negative intensities when applied to the general Legendre phase-function, requiring correction of radiation intensity during computation processes.

3) Hunter and Guo's 2012 normalization is able to conserve both scattered energy and average angle simultaneously, drastically improving radiative transfer modelling accuracy with respect to Monte Carlo. Application of this technique is slightly more complicated than Mishchenko's E or Kamdem Tagne's g, as solution of a matrix equation is necessary. Every phase-function value in the system is normalized, and no negative intensity correction is necessary for diffuse radiation. For ballistic radiation, correction is only necessary for the lowest direction number.

4) Hunter and Guo's 2014 normalization conserves both scattered energy and average angle in a mathematically simple manner. For HG phase-functions and diffuse radiation, no negative intensity correction is required, and radiative transfer predictions are of equal accuracy as Hunter and Guo's 2012 normalization, making it a simple yet desirable technique. For Legendre phase-functions in diffuse radiation, and ballistic radiation regardless of phase function type, however, negative intensities are encountered frequently and its usefulness is limited.

5) As a general guideline, Hunter and Guo's 2014 normalization is the best for diffuse radiation transfer using monotonic phase-functions (such as HG approximation), although use of negative intensity correction allows for radiative transfer accuracy in other situations. Hunter and Guo's 2012 normalization is the most desirable approach when general Legendre polynomial phase-functions are used, and also for ballistic radiation, as it avoids negative intensities for all but the lowest directional order.

6) The DOM, in terms of its ability to reduce both computational memory and CPU convergence times, is a more computationally efficient method than the FVM. The limitation of quadratures with DOM has been resolved by the recent development of high-order quadrature schemes. Certainly the FVM does offer more quadrature flexibility.

7) Radiative transfer results using both the DOM and FVM when both scattered energy and asymmetry factor are conserved are accurate to MC and are on the same order of accuracy to each other.

REFERENCES

[1] Edwards D.K., and Balakrishnan A., Thermal radiation by combustion gases, *International Journal of Heat and Mass Transfer*, vol. 16, 1973, pp. 25-40.

[2] Tien C.L., and Lee S.C., Flame radiation, *Progress in Energy and Combustion Science*, vol. 8, 1982, pp. 41-59.

[3] Taine J., and Soufiani A., Gas IR radiative properties: from spectroscopic data to approximate models, *Advances in Heat Transfer*, vol. 33, 1999, pp. 295-414.

[4] Howell J.R., and Siegel R., *Thermal Radiation Heat Transfer*, 4th ed., Taylor & Francis: New York, 2002.

[5] Modest M.F., *Radiative Heat Transfer*, 2nd ed., Academic Press: New York, 2003.

[6] Solovjov V.P., and Webb, B.W., An efficient method for modeling radiative transfer in multicomponent gas mixtures with soot, *Journal of Heat Transfer,* Vol. 123, 2001, pp. 450-457.

[7] Tuncer O., Acharya S., and Uhm, J.H., NO_x and flashback characteristics of confined premixed hydrogen-enriched methane flames, *International Journal of Hydrogen Energy,* Vol. 34, 2009, pp. 496-506.

[8] Seo T, Kaminski D.A.., and Jensen, M.K., Combined convection and radiation in simultaneously developing flow and heat transfer with nongray gas mixtures, *Numerical Heat Transfer A,* Vol. 26, 2002, pp. 49-66

[9] Guo Z., and Maruyama S., Radiative heat transfer in nonhomogeneous, nongray, and anisotropic scattering media, *International Journal of Heat and Mass Transfer,* Vol. 43, 2000, pp. 2325-2336.

[10] Guo Z., Maruyama S., and Tagawa S., Combined heat transfer in floating zone growth of large silicon crystals with radiation on diffuse and specular surfaces, *Journal of Crystal Growth*, Vol. 194, 1998, pp. 321-330.

[11] Chen C., and Jaluria, Y., Modeling of radiation heat transfer in the drawing of an optical fiber with multilayer structure, *Journal of Heat Transfer,* Vol. 129, 2007, pp. 342-352.

[12] de Ris J., Fire radiation – A review, *17th Symposium (International) on Combustion*, Vol. 17, 1979, pp. 1003-1016.

[13] Shokri M., and Beyler C.L., Radiation from large pool fires, *Journal of Fire Protection Engineering*, Vol. 1, 1989, pp. 141-149.

[14] Albini F.A., A model for fire spread in wildland fuels by radiation, *Combustion Science and Technology*, Vol. 42, 1985, pp. 229-258.

[15] Cumber, P.S., Ray effect mitigation in jet fire radiation modeling, *International Journal of Heat and Mass Transfer*, Vol. 43, 2000, pp. 935-943.
[16] Goody R.M., and Yung Y.L., Atmospheric radiation: Theoretical basis, Oxford University Press, 1995.
[17] Bliss R.W., Atmospheric radiation near the surface of the ground: a summary for engineers, *Solar Energy*, Vol. 5, 1961, pp. 103-120.
[18] Angstrom, A., Solar and terrestrial radiation: Report to the international commission for solar research on actinometric investigations of solar and atmospheric radiation, *Quarterly Journal of the Royal Meteorological Society*, Vol. 50, 1924, pp. 121-126.
[19] Elsasser, W.M., Heat transfer by infrared radiation in the atmosphere, Harvard University: Blue Hill Meterological Observatory, 1942.
[20] Gratzel M., Mesoscopic solar cells for electricity and hydrogen production from sunlight, *Chemistry Letters*, Vol. 34, 2005, pp. 8-13.
[21] Turner J.A., A realizable renewable energy future, *Science 30*, Vol. 285, no. 5428, 1999, pp. 687-689.
[22] Tzen E., and Morris R., Renewable energy sources for desalination, *Solar Energy*, Vol. 75, 2003, pp. 375-379.
[23] Cucinotta F.A., and Durante M., Cancer risk from exposure to galactic cosmic rays: implications for space exploration by human beings, *The Lancet Oncology*, Vol. 7, 2006, pp. 431-435.
[24] Gordon W.E., Incoherent scattering of radio waves by free electrons with applications to space exploration by radar, *Proceedings of the IRE*, Vol. 46, 1958, pp. 1824-1829.
[25] Durante M., and Cucinotta A., Heavy ion carcinogenesis and human space exploration, *Nature Reviews Cancer*, Vol. 8, 2008, pp. 465-472.
[26] Kumar S., and Mitra K., Microscale aspects of thermal radiation transport and laser applications, *Advances in Heat Transfer*, vol. 33, 1999, pp.187-294.
[27] Hatano M., Moon S., Lee M., Suzuki K., and Grigoropoulos C.P., Excimer laser-induced temperature field in melting and resolidification of silicon thin films, Journal of Applied Physics, Vol. 87, 2000, pp. 36-43
[28] Choi T.Y., and Grigoropoulos C.P., Plasma and ablation dynamics in ultrafast laser processing of crystalline silicon, Journal of applied physics, Vol. 92, 2002, pp. 4918-4925
[29] Yamada Y., Light-tissue interaction and optical imaging in biomedicine, *Annual Review on Heat Transfer*, Vol. 6, 1995, pp. 1-59.
[30] Kim B.-M., Feit M.D., Rubenchik A.M., Joslin E.M., Celliers P.M., Eichler J. et al., Influence of pulse duration on ultrashort laser pulse ablation of biological tissues, *Journal of Biomedical Optics*, Vol. 6, 2001, pp. 332-338.
[31] Huang H., and Guo Z., Ultrashort pulsed laser ablation and stripping of freeze-dried dermis, *Lasers in Medical Science,* Vol. 25, 2010, pp. 517-524.
[32] Guo Z., Wang X.L., and Huan H., Plasma-mediated ablation of biofilm contamination, *Applied Surface Science*, Vol. 257, 2010, pp. 1247-1253.
[33] Jaunich M, Raje S., Kim K.H., Mitra K., and Guo Z., Bio-heat transfer analysis during short pulse irradiation of tissues, *International Journal of Heat and Mass Transfer*, Vol. 51, 2008, pp. 5511-5521.
[34] Jiao J., and Guo Z., Modeling of ultrashort pulsed laser ablation in water and biological tissues in cylindrical coordinates, *Applied Physics B*, Vol. 103, 2001, pp. 195-205.
[35] Bass L.S., and Treat M.R., Laser tissue welding: a comprehensive review of current and future applications, *Lasers in Surgery and Medicine*, Vol. 17, 1995, pp. 315-349.
[36] Kim K.H., and Guo Z., Ultrafast radiation heat transfer in laser tissue welding and soldering, *Numerical Heat Transfer A*, Vol. 46, 2004, pp. 23-40.
[37] Sajjadi A.Y., Mitra K., and Guo Z., Thermal analysis and experiments of laser–tissue interactions: A review, *Heat Transfer Research*, vol. 44, 2013, pp. 345-388.
[38] Guo Z., and Hunter B., Advances in ultrafast radiative transfer modeling and applications: A review, *Heat Transfer Research* vol. 44, 2013, pp. 303-344.
[39] Raithby G.D., and Chui E.H., A finite-volume method for predicting a radiant heat transfer in enclosures with participating media, *Journal of Heat Transfer*, Vol. 112, 1990, pp. 415-423.
[40] Chui E.H., Raithby G.D., and Hughes P.M.J., Prediction of radiative transfer in cylindrical enclosures with the finite volume method, *Journal of Thermophysics and Heat Transfer*, Vol. 6, 1992, pp. 605-611.
[41] Chui E.J., Hughes P.M.J., and Raithby G.D., Implementation of the finite-volume method for calculating radiative transfer in a pulverized fuel flame, *Combustion Science and Technology*, Vol. 92, 1993, pp. 225-242.
[42] Murthy J.Y., and Mathur S.R., Finite volume method for radiative heat transfer using unstructured meshes, *Journal of Thermophysics and Heat Transfer*, Vol. 12, 1998, pp. 313-321.
[43] Chai J.C., Lee H.S., and Patankar S.V., Finite volume method for radiation heat transfer, *Journal of Thermophysics and Heat Transfer*, Vol. 8, 1994, pp. 419-425.
[44] Chai J.C., Hsu P.-f., and Lam Y.C., Three-dimensional transient radiative transfer modeling using the finite-volume method, *Journal of Quantitative Spectroscopy and Radiative Transfer*, Vol. 86, 2004, pp. 299-313.
[45] Hunter B., and Guo Z., Comparison of discrete-ordinates method and finite volume method for steady-state and ultrafast radiative transfer analysis in cylindrical coordinates, *Numerical Heat Transfer B*, Vol. 59, 2011, pp. 339-359.
[46] Fiveland W.A., Discrete-ordinates solutions of the radiative transport equation for rectangular enclosures, *Journal of Heat Transfer*, Vol. 106, 1984, pp. 699-706.
[47] Fiveland W.A., Three dimensional radiative heat transfer solution by the discrete-ordinates method, *Journal of Thermophysics and Heat Transfer*, Vol. 2, 1988, pp. 309-316.
[48] Guo Z., and Kumar S., Discrete-ordinates solution of short-pulsed laser transport in two-dimensional turbid media, *Applied Optics*, Vol. 40, 2001, pp. 3156-3163.
[49] Guo Z., and Kumar S., Three-dimensional discrete ordinates method in transient radiative transfer, *Journal of Thermophysics and Heat Transfer*, Vol. 16, 2002, pp. 289-296.
[50] Chai J.C., Lee H.S., and Patankar S.V., Ray effect and false scattering in the discrete ordinates method, *Numerical Heat Transfer B*, Vol. 24, 1993, pp. 373-389.
[51] Coelho P.J., The role of ray effects and false scattering on the accuracy of the standard and modified discrete ordinates methods, *Journal of Quantitative Spectroscopy and Radiative Transfer*, Vol. 73, 2002, pp. 231-238.
[52] Coelho P.J., Bounded skew high-order resolution schemes for the discrete ordinates method, *Journal of Computational Physics*, Vol. 175, 2002, pp. 412-437.
[53] Jessee J.P., and Fiveland W.A., Bounded, high-resolution differencing schemes applied to the discrete ordinates method, *Journal of Thermophysics and Heat Transfer*, Vol. 11, 1997, pp. 540-548.
[54] Coelho P.J., Bounded skew high-order resolution schemes for the discrete ordinates method, Journal of Computational Physics, Vol. 175, 2002, pp. 412-437.

[55] Hunter B., and Guo Z., Conservation of asymmetry factor in phase function discretization for radiative transfer analysis in anisotropic scattering media, *International Journal of Heat and Mass Transfer*, Vol. 55, 2012, pp. 1544-1552.

[56] Hunter B., and Guo Z., Reduction of angle splitting and computational time for the finite volume method via phase function normalization, *International Journal of Heat and Mass Transfer*, Vol. 55, 2012, pp. 2449-2460.

[57] Hunter B., and Guo Z., Phase-function normalization in 3-D discrete-ordinates solution of radiative transfer – Part I: Conservation of scattered energy and asymmetry factor, *Numerical Heat Transfer B*, Vol. 62, 2012, pp. 203-222.

[58] Hunter B., and Guo Z., Phase-function normalization in 3-D discrete-ordinates solution of radiative transfer – Part II: Benchmark comparisons, *Numerical Heat Transfer B*, Vol. 62, 2012, pp. 223-242.

[59] Hunter B., and Guo Z., A new and simple technique to normalize HG phase function for conserving scattered energy and asymmetry factor, *Numerical Heat Transfer B*, Vol. 65, pp. 195-217, 2014.

[60] Kim T.K., and Lee H., Effect of anisotropic scattering on radiative heat transfer in two-dimensional rectangular enclosures, *International Journal of Heat and Mass Transfer*, Vol. 31, 1988, pp. 1711-1721.

[61] Crosbie A.L., and Schrenker R.G., Radiative transfer in two-dimensional rectangular medium exposed to diffuse radiation, *Journal of Quantitative Spectroscopy and Radiative Transfer*, Vol. 31, 1984, pp. 339-372.

[62] Boulet P., Collin A., and Consalvi J.L., On the finite volume method and the discrete ordinates method regarding radiative heat transfer in acute forward anisotropic scattering media, *Journal of Quantitative Spectroscopy and Radiative Transfer*, Vol. 104, 2007, pp. 460-473.

[63] Collin A., Consalvi J.L., and Boulet P., Acute anisotropic scattering in a medium under collimated irradiation, *International Journal of Thermal Sciences*, Vol. 50, 2011, pp. 19-24.

[64] Longoni G., and Haghighat A., Development of new quadrature sets with the "ordinate splitting" technique, *Proceedings of the ANS International Meeting on Mathematical Methods for Nuclear Applications*, 2001, Salt Lake City, Utah.

[65] Endo T., and Yamamoto A., Development of new solid angle quadrature sets to satisfy even- and odd-moment conditions, *Journal of Nuclear Science and Technology*, Vol. 44, 2007, pp. 1249-1258.

[66] Carlson B.G., Tables of symmetric equal-weight quadrature EQ_N over the unit sphere, Los Alamos Scientific Laboratory Report LA-4734, Los Alamos, New Mexico, 1971.

[67] Thurgood C.P., Pollard A., and Becker H.A., The T_N quadrature set for the discrete ordinates method, *Journal of Heat Transfer*, Vol. 117, 1995, pp. 1068-1070.

[68] Li B-W., Yao Q., Cao X-Y., and Cen K-F., A new discrete ordinates quadrature scheme for three-dimensional radiative heat transfer, *Journal of Heat Transfer*, Vol. 120, 1998, pp. 514-518.

[69] Hunter B., and Guo Z., Comparison of quadrature schemes in DOM for anisotropic scattering radiative transfer analysis, *Numerical Heat Transfer, Part B: Fundamentals*, vol. 63, 2013, pp. 485-507.

[70] Kim S.H., and Huh K.Y., A new angular discretization scheme of the finite volume method for 3-D radiative heat transfer in absorbing, emitting, and anisotropically scattering media, *International Journal of Heat and Mass Transfer*, Vol. 43, 2000, pp. 1233-1242.

[71] Lee H., and Buckius R.O., Scaling anisotropic scattering in radiation heat transfer for a planar medium, *Journal of Heat Transfer*, vol.104, 1982, pp. 68–75.

[72] Kim T.K., and Lee H.S., Scaled isotropic results for two dimensional anisotropic scattering media, *Journal of Heat Transfer*, vol. 112, 1990, pp. 721–727.

[73] Guo Z., and Maruyama S., Scaling anisotropic scattering in radiative transfer in three-dimensional nonhomogeneous media, *International Communications on Heat and Mass Transfer*, Vol. 26, 1999, pp. 997-1007.

[74] Guo Z., and Kumar S., Equivalent isotropic scattering formulation for transient short-pulse radiative transfer in anisotropic scattering planar media, *Applied Optics*, Vol. 39, 2000, pp. 4411-4417.

[75] Mishchenko M.I., Dlugach J.M., Vanovitskij E.G., and Zakharova N.T., Bidirectional reflectance of flat, optically thick particulate layers: an efficient radiative transfer solution and applications to snow and soil surfaces, *Journal of Quantitative Spectroscopy and Radiative Transfer*, Vol. 63, 1999, pp. 409-432.

[76] Kamdem Tagne, H.T., Phase function normalization in discrete ordinate method, *submitted for review*, 2013.

[77] Hunter B., and Guo Z., Improved treatment of anisotropic scattering in radiation transfer analysis using the finite volume method, *Heat Transfer Engineering*, *accepted*, 2014.

[78] Cheong W.F., Prahl S.A., and Welch A.J., A review of the optical properties of biological tissue, *IEEE Journal of Quantum Electronics*, Vol. 26, 1990, pp. 2166-2185.